UNIVERSIDADE FEDERAL DO CEARÁ
CENTRO DE CIÊNCIAS
DEPARTAMENTO DE FÍSICA
PROGRAMA DE PÓS-GRADUAÇÃO EM FÍSICA

JUAN SIMON RODRIGUEZ HERNANDEZ

Structural phase transitions on hybrid organic-inorganic halide perovskites based on bromide

Orientation by: Carlos William de Araujo Paschoal
Co-orientation by: Dieric dos Santos de Abreu

FORTALEZA-CE
2019

JUAN SIMÓN RODRÍGUEZ HERNÁNDEZ

STRUCTURAL PHASE TRANSITIONS ON HYBRID ORGANIC-INORGANIC HALIDE PEROVSKITES BASED ON BROMIDE

Master thesis presented to the Post-Graduation Program in Physics of the Federal University of Ceará as part of the partial requisites to obtain the Master Degree in Physics. Area of concentration Condensed Matter Physics.

Advisor: Prof. Dr. Carlos William de Araújo Paschoal

Co-Advisor: Dr. Dieric dos Santos de Abreu

FORTALEZA

2019

Dados Internacionais de Catalogação na Publicação
Universidade Federal do Ceará
Biblioteca Universitária
Gerada automaticamente pelo módulo Catalog, mediante os dados fornecidos pelo(a) autor(a)

R618s Rodríguez Hernández, Juan Simon.
Structural phase transitions on hybrid organic-inorganic halide perovskites based on bromide / Juan Simon Rodríguez Hernández. – 2019.
63 f. : il. color.

Dissertação (mestrado) – Universidade Federal do Ceará, Centro de Ciências, Programa de Pós-Graduação em Física, Fortaleza, 2019.
Orientação: Prof. Dr. Carlos William de Araujo Paschoal.
Coorientação: Prof. Dr. Dieric dos Santos de Abreu.

1. Halide inorganic-organic perovskite. 2. Phase Crystal Transition. 3. Order-disorder Mechanics. 4. Low-temperature variation. 5. Raman spectroscopy. I. Título.

CDD 530

JUAN SIMÓN RODRÍGUEZ HERNÁNDEZ

STRUCTURAL PHASE TRANSITIONS ON HYBRID ORGANIC-INORGANIC HALIDE PEROVSKITES BASED ON BROMIDE

A master thesis presented to the Post-Graduation Program in Physics of the Federal University of Ceará as part of the partial requisites to obtain the Master Degree in Physics. Area of concentration Condensed Matter Physics.

Approved on: 01/03/2019

EXAMINATION JUDGES

_____

Prof. Dr. Carlos William de Araújo Paschoal (Advisor)
Universidade Federal do Ceará (UFC)
Physics Departament

_____

Dr. Dieric Dos Santos de Abreu (Co-Advisor)
Universidade Federal do Ceará (UFC)
Physics Departament

_____

Prof. Dr. Gilberto Dantas Saraiva
Universidade Estadual do Ceará (UECE)
Physics Departament

_____

Prof. Dr. Pierre Basílio Almeida Fechine
Universidade Federal do Ceará (UFC)
Chemestry Departament

Acknowledgements

First, I would like to thank my advisor Professor Carlos William de Araújo Paschoal for having accepted me as his master student, proposed me this project, let me be part of his research group, suggest and guide me during the investigation. Thank you Professor for the patience and this good opportunity.

I like to thank also my co-advisor, Dieric dos Santos de Abreu for his helpful chemistry hands, advice and suggestions in all investigation.

I would like to express my appreciation to the members of the Jury, Professor Gilberto Dantas Saraiva and Professor Pierre Basílio Almeida Fechine for the corrections, comments, and suggestions. This appreciation also goes to Professors Alejandro Ayala, José Alves de Lima Jr, and Paulo de Tarso because they helped me during the analysis of techniques involved in this work.

I very grateful with Dr. Manuel Andujar, Rosivaldo and Ariel for the $DMAPbBr_3$ sample.

Thanks to all members of FEMM and LabCrEs groups for all the support.

Many thanks to Wendell and Mayra for the help with the DSC and X-ray diffraction measurements.

A special acknowledgment to my friends, Wendell, Felipe, Pedro, Thiago, Enzo and Natalia for supporting me.

I would like to thank my family, my parents Flor and Yovanny and my brother Jesus for everything, despite; the distance is incredible. I know you always support me. I am very proud to represent them.

Also, I would thank my grandparents, uncles, cousins, parents in law and friends in Venezuela.

Thanks to Mayra, my both left and right hand, my partner, girlfriend, friend, and everything, thank you very much for always pushing me to be a better person, to focus me and made my days bright. I know that together we can reach all goals.

Thanks to the UFC and Post-Graduation for giving me the opportunity to study my master degree here in Brazil. Finally, I would like to thanks CNPq, CAPES, and FUNCAP for financial support.

This study was financed in part by the Coordenação de Aperfeiçoamento de Pessoal de Nível Superior - Brasil (CAPES) - Finance Code 001

Abstract

Halide inorganic-organic perovskite (HIOP) are promising new functional materials for solar cell applications as other optoelectronic performance such as light emitting diodes, low-threshold lasers, and photodetectors. The halide modification in the perovskite crystal structure represented in the material different applications and properties, important research groups and industries today are seeking organics replacement in the crystal composition. One of the natural changes is the dimethylammonium $[(CH_3)_2NH_2]^+$ (DMA) organic cation because is highly responsible for ordering in the crystal structure, and in most cases responsible for the ferroelectric order. In this context, we discuss with a DFT calculation the vibrational assignation in the DMA molecule for a modest attribution, also we have prepared with the bromide halide and DMA two perovskites compositions by using simple lab conditions at room temperature. These compounds exhibit a phase crystal transition, where the order-disorder mechanics act. One of synthesized material is the hexagonal three-dimensional $DMAPbBr_3$ perovskite; we found with our X-ray diffraction, differential scanning calorimetric and Raman spectroscopy measurements at 250 K a phase crystal transition for hexagonal to an orthorhombic system. On the other hand, we described with Raman spectroscopy in low-temperature the isostructural phase transition of two-dimensional $DMA_7Pb_4Br_{15}$, in both compounds, the stretching H-bond in the CH_3 groups at high frequencies is the ones who are responsible for the ordering in DMA organic cation. These materials not only open large possibilities and applications of differences electrical and optical properties, but they also have advantages as an easy synthesized method and cheap materials and low-temperature formation.

Keywords: Halide inorganic-organic perovskite, phase crystal transition, order-disorder mechanics, low-temperature variation, X-ray diffraction, Raman spectroscopy.

Resumo

Perovskitas de haleto inorgânico-orgânico (HIOP) é um novo material funcional promissor para aplicações em células solares, assim como outros desempenhos optoeletrônicos, como diodos emissores de luz, lasers de baixo patamar e fotodetectores. A modificação do haleto na estrutura cristalina da perovskita acarreta em diferentes aplicações e propriedades do material, grupos de pesquisa e indústrias, atualmente, buscam não apenas uma substituição de haletos, mas também uma substituição da parte orgânica na composição dos cristais. É comum realizar a troca do cátion orgânico por dimetilamônio $[(CH_3)_2NH_2]^+$ (DMA), pois ele é responsável pela ordem ferroelétrica. Neste contexto, nos disociamos com um calculo de DFT os modos vibracionaes na molecula de DMA para uma atribucao modesta, alem preparamos duas composições de perovskitas com haleto de brometo e DMA usando os aparatos laboratoriais em condições ambientes. Estes compostos exibem uma transição de fase cristalina, onde a mecânica de ordem e desordem age. Um dos materiais sintetizados foi a perovskita tridimensional $DMAPbBr_3$; com as análises de DRX, DSC e Raman encontramos uma transição de fase do sistema hexagonal a temperatura ambiente para ortorrômbico em 250 K. Por outro lado, com a espectroscopia Raman em baixa temperatura foi exibida uma transição de fase isoestrutural a 250 K na segunda composição denominada de $DMA_7Pb_4Br_{15}$. Em ambos compostos, os componentes de ligação H do grupo CH_3 em altas frequências são os responsáveis da ordenação do cátion orgânico DMA. Estes materiais não só abrem grandes possibilidades para aplicações elétricas e ópticas como também apresentam uma síntese, relativamente, simples, rápida, com materiais baratos e em baixa temperatura.

Palavras chave: Perovskitas de haleto inorgânico-orgânica, transição de fase cristalina, mecânica de ordem-desordem, variação de baixa temperatura, difração de raios-X, espectroscopia Raman.

List of Figures

List of Tables

Contents

Introduction

One of the most important challenges for society is made efficient devices in order to decrease energy demand. In the beginner of this century solving this problem, important research groups, as well as private companies, have seen with great importance the investigation and production of solar cells. This study has developed rapidly and currently is one the trending topic in physics and materials science. One of the promising prospects for this employment is the materials with perovskite crystal structure because they have a high power conversion of 22.7 % that has been achieved within the short time of their development. (HUANG et al., 2017) All this evolution is highlight in Figure 1, where is described the increment in the device efficiency to power conversion of sunlight in electricity using this type of compounds for two different rates: (a) validated data by the National Renewable Energy Laboratory in a period of 2009 until 2014 (MCGEHEE, 2014) and (b) from 2013 to 2018. (LI et al., 2018b)

Figure 1: (a) The world record power-conversion efficiency of perovskite solar cells over time. Earlier data points were reported in the literature, but not validated. More recent data have all been validated by the National Renewable Energy Laboratory. (MCGEHEE, 2014) (b) Increase in the power conversion efficiency (PCE) of perovskite solar cells (PSCs) with different device areas: small-area cells (pink), large-area cells (blue) and modules (grey) during the year range of 2013-2018. (LI et al., 2018b)

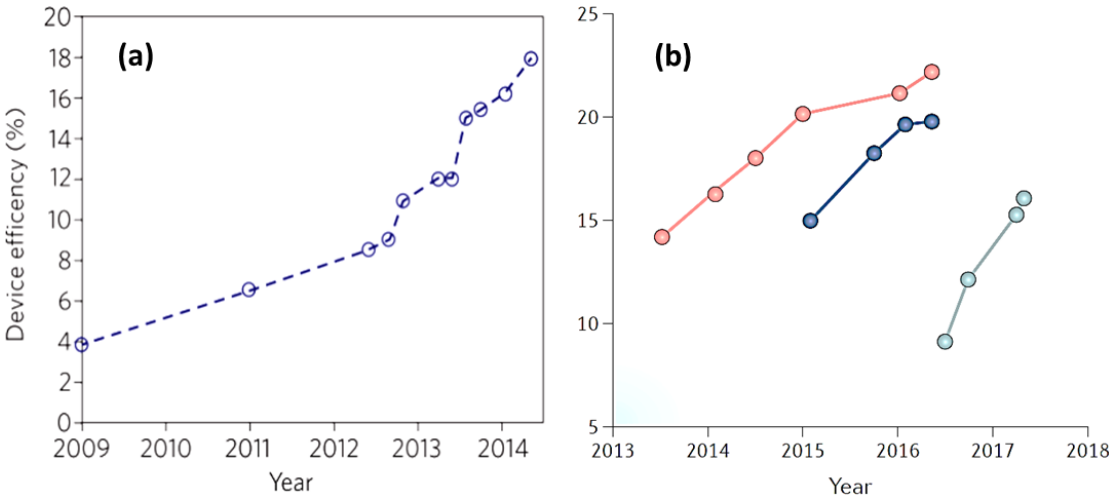

Another advantage that these type materials have is the low-cost production, nature-abundant raw elements, low growing temperature, and scalable solution fabrication processes. Also these compounds attract remarkable characteristics for is high absorption appreciations as notable hole-electron electronic transitions and also for exhibits exceptional high efficiency. (HAO et al., 2014; LI et al., 2017) Among include

superconductivity, magnetoresistance, ionic conductivity, and a multitude of dielectric properties. As well they have excellent optoelectronic properties, fault tolerance, sharp band edge, and tunable band range across the visible and near-infrared range. (SALIBA et al., 2018)

In this particular, the perovskites have a numerous quantity of investigations in the scientific community to improve devices with good stability, efficiency and low toxicity that are the current issues in this type of compounds. In order to make better materials the research is flared in hybrid perovskites compounds, even though, the understanding of some physical properties is still unclear. This work aims some characterization about the structural phase transition (SPT) in hybrid organic-inorganic perovskites (HIOP) based in dimethylammonium (DMA) and bromide halide namely as $DMAPbBr_3$ and $DMA_7Pb_4Br_{15}$ crystals. In the opening chapter is describe a review of hybrid perovskites compounds, after discuss the experimental method to investigate both samples. Next, is characterize the SPT in the three-dimensional $DMAPbBr_3$ perovskite at low temperatures by Raman spectroscopy, single-crystal X-ray diffraction, and differential scanning calorimetry and following, is show the Raman spectroscopy measurements of the $DMA_7Pb_4Br_{15}$ crystal.

Chapter 1: Organic-inorganic halide perovskites

The purpose of this chapter is described some of the most important properties and possible applications of the organic-inorganic halide perovskites. In this particular, we emphasize in a survey of these compounds and discuss some physical properties that are still debated in the actual, which will have a greater depth in the perovskites based in different halides and DMA organic molecule. Thus, we begin with the perovskite crystal structure.

1.1. The perovskite crystal structure

The term *"perovskite"* is commonly used to referring a large group of compounds with a crystal structure resembling the mineral calcium titanium oxide ($CaTiO_3$). (PETROVIĆ; CHELLAPPAN; RAMAKRISHNA, 2015) Such compounds have a stoichiometric formula ABX_3, in which the A cations are in dodecahedral sites, and the B cations are in octahedral sites. In the ideal case, perovskites have a cubic unit cell, with the B cation at the cube corners, and A cation at the center of the cell coordinated to six X anions at the center of the cube faces, as it is shown in Figure 2. Thus, in an ideal cubic perovskite, the BX_6 octahedra form a 3D octahedral network. This structure has cubic symmetry and belongs to the $Pm\bar{3}m$ (O_h^1) space group. (BAY et al., 2017)

Figure 2: Ideal cubic ABX_3 perovskite structure representation with the coordination of A- (blue), B- (green) and X- (red) sites.

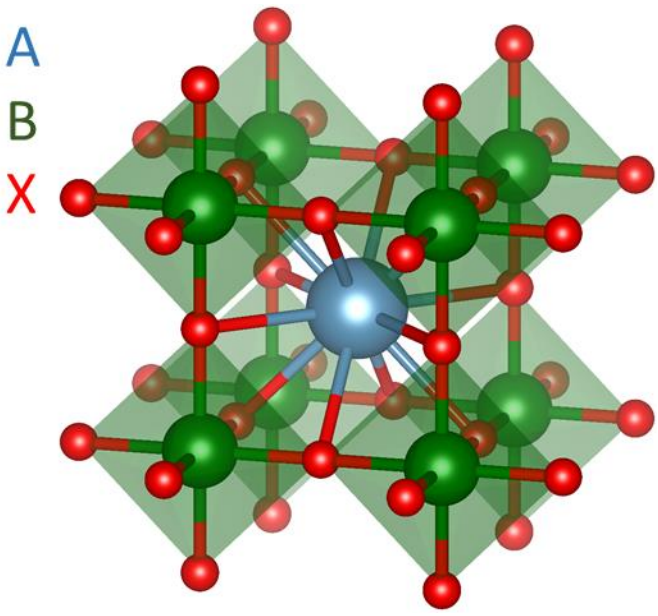

Even though the basic structure of perovskite is relatively simple, there are still some large numbers of different and possible structural variations among them, because the A and B cations can accommodate virtually any element in the periodic table, while anions can be oxygen, fluorine, hydroxyl, and so on. These combinations allow a vast variety of materials with distinct, interesting physical properties and diverse technological applications, being perovskites one of the most complex oxides employed by device industries. (BHALLA; GUO; ROY, 2000)

Such substitutions lead to new properties, but also, usually, they lead to different crystalline structures too, which derives from the ideal cubic perovskite. The relative ionic size is an essential requirement for the stability of the structure, so distortion in the arrangement can produce several lower-symmetry distorted. (LI et al., 2018a) The Goldschmidt tolerance factor (T) for perovskite compounds (ABX_3) is a rigid ion model for evaluating crystalline structures in terms of their geometric stability and distortion based on the ionic packing. It is defined as the ratio of constituent ionic radii of A, B and X as

$$\boldsymbol{T = \frac{1}{\sqrt{2}} \frac{(r_A + r_X)}{(r_B + r_X)}} \quad \textbf{(1)}$$

where r_A, r_B and r_x are the ionic radii of A, B and X ions, respectively. (SATO et al., 2016) In the case $t = 1$ the composition has the crystal cubic close packed structure (Figure 2). When the ratio of the ionic radii deviates from the ideal value ($t \neq 1$), a geometric strain and crystal distortions arise giving origin to different symmetries, being hexagonal, tetragonal, orthorhombic and monoclinic phases are the most common non-cubic variants. (SATO et al., 2016; TILLEY, 2016)

1.2. Perovskites applications

In the last decade, the importance of perovskite compounds has been increasing still more, since the discovery of their photovoltaic properties when they are based on halide anions. Due to the intense search for clean energy sources for sustainability and environment requirements, the investigations on such perovskites have developed rapidly and, currently, are one the trending topic in physics and materials science. One of the forecasts for their applications is the increase in the device efficiency and power conversion of sunlight into electricity using this kind of compounds. The impact of halide

perovskite compounds has increased due to the discoveries and novel device concepts for application into solar cells purposes based on inorganic-organic hybrid halide perovskites. (GRÄTZEL, 2014) Such compounds in the photovoltaic research community are highly investigated because, in addition to the high power conversion efficiencies (22.7%) that have been achieved within the short time of their development, (HUANG et al., 2017) they have low-cost production (MCGEHEE, 2013), nature-abundant raw elements, low growth temperature, and scalable solution fabrication processes. Thus, these devices are the ultimate goal of the solar-cell industry, because these devices could be the key to induce a clear alternative to the current methods of generating energy. (GRÄTZEL, 2001; ZHANG; YIN, 2018) Halide perovskites are composed by a halide, fluoride, chloride, bromide or iodide (F, Cl, Br or I). Among these features, these compounds attract unusual characteristics for their notable hole-electron electronic transitions and also to exhibit exceptional high efficiency. (HAO et al., 2014; LI et al., 2017) This type of materials includes superconductivity, magnetoresistance, ionic conductivity, and a multitude of dielectric properties. As well they have excellent optoelectronic properties, fault tolerance, sharp band edge, and tunable band range across the visible and near-infrared range. (SALIBA et al., 2018)

In the physical point view, the promise of these hybrid materials derives from the confluence of several factors, which include very high optical absorption, small effective masses for electrons and holes, dominant point defects that generate shallow levels, and grain boundaries. (SAPAROV; MITZI, 2016) Also, these compositions have very long electron-hole diffusion lengths, tunable bandgap, unusually long charge carrier lifetimes, small exciton binding energies, in some cases high photoluminescence, narrow emission linewidth that made them an novel compound for electric properties, as well enabling promising optoelectronic applications, such as light-emitting diodes, low-threshold lasers and photodetectors. (YIN et al., 2017) Thus, since the perovskite structure permits several substitutions, the search for new halide perovskites has been intense. Several investigations show that using different halide contents lead to changes in the inorganic metal-halide network as well as the change of the organic anion. Theoretical results involving such substitutions show that it is possible to obtain new hybrid lead halide perovskites with the basic crystal structure ABX_3 or different octahedral network based on perovskites. (BECKER; KLÜNER; WARK, 2017; QIAN et al., 2017; TSAI et al., 2016)

1.3. Octahedral perovskites arrays dimensions

A simple way for understanding this kind of crystalline changes is to classify the new phase crystalline structures according to the spatial arrangement of the octahedra metal halide units (BX_6). Observe that the structure is not strictly a perovskite, but is common the literature calls such structure by perovskites because such structure is always used as a reference. Thus, we can call three (3D), two (2D), one (1D) and zero (0D) type structures due to the dimensional octahedral arrays. (LIN et al., 2018) In Figure 3 are described the typical 3D, 2D, 1D, and 0D perovskite-like crystalline structures. Each kind of materials has unique physical and chemical properties with a variety of potential applications. As we showed in Figure 3, the 3D halide perovskites are bulk materials with chemical formula ABX_3 that consist of frameworks with corner-sharing metal halide octahedra that extend in all three dimensions, with small cations fitting into the void spaces between the octahedral. (LIN et al., 2018) The 2D perovskites structures are considered as sheets, layers or planes ripped in a specific crystallographic direction. These layered materials have a general chemical formula $A_{m-1}A'_2B_mX_{3m-1}$, where A' is an alkyl, A is a metal cation, X is a halide, and the variable m indicates the number of the metal cation layers between the two layers of the organic chains.

Figure 3: Typical structure of 3D, 2D, 1D and 0D perovskites (red spheres: metal centers; green spheres: halide atoms; blue spheres: nitrogen atoms; gray spheres: carbon atoms; orange spheres: oxygen atoms; purple polyhedrons: metal halide octahedra; hydrogen atoms are hidden for clarity).(LIN et al., 2018)

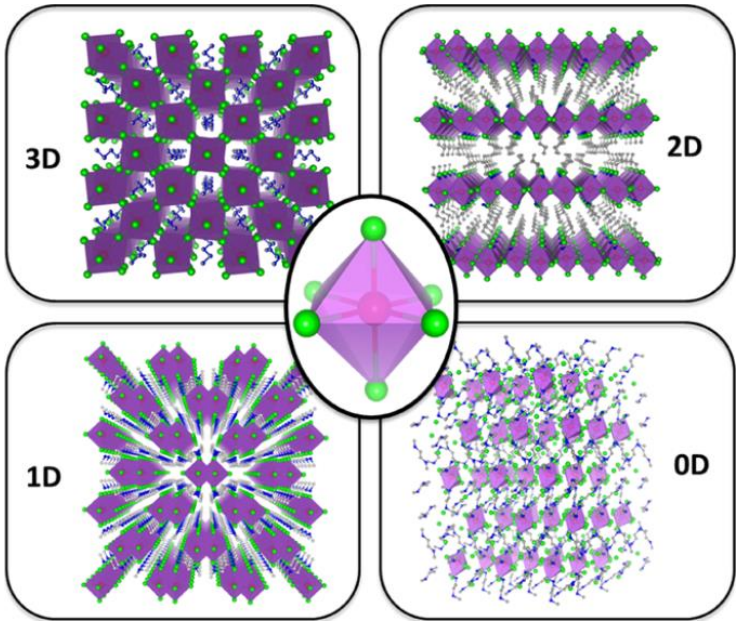

One of the hybrid halide perovskites that have gained significant attention today is the methylammonium lead iodide $CH_3NH_3PbI_3$ (A=MA=CH_3NH_3; B=Pb; X=I). This hybrid perovskite, which is obtained by simple solution-based processing at low temperature, exhibits strong optical absorption and the highest power conversion efficiency (PCE >20%) showed today. Such values are comparable with the best thin-film solar cells based on Cu(In, Ga)Se_2 or CdTe. (EAMES et al., 2015) Another important halide perovskite is the chlorine-based $MAPbCl_3$, which have attracted an immense interest recently as an excellent candidate for photovoltaic solar cells. However, its maximum PCE is 19.3%, although it has a large absorption coefficient in the visible–near-infrared spectral range, and high charge carriers photogeneration efficiency. Both properties are excellent for photovoltaic applications. (ZHANG et al., 2015) $MAPbBr_3$ also has outstanding properties as a single crystal, such ultralow defect densities (below 10^{11} cm^{-3}), extremely long carrier lifetimes (up to 15 μs) and diffusion lengths (above 175 μm), which have been determined from combinations of optical and electronic measurements. (WENGER et al., 2017a)

Despite the multiple ionic compositions that have been reported, the organic cation present in the structure constitutes an important feature for high-efficiency formulations. Thus, several investigations are focused on the substitution in this site for several molecules to find crystal structures with excellent properties. The common molecules employed are dimethylammonium (DMA), ethylammonium (EA), guanidium (G), formamidinium (FA) and trimethylammonium (TMA) cations. The synthesis of new crystals and their characterizations represent a step forward to understand the hybrid perovskites. Thus, $APbX_3$ systems with X=I, Br and Cl, and A=DMA and TMA were investigated and showed higher optical band-gaps concerning the MA-based family. (MANCINI et al., 2016) Also, a new layered compound (2D perovskite structure) $FAGPbI_4$ was also studied and exhibits a strong photoluminescent (PL), besides pronounced photoconductivity. (NAZARENKO et al., 2018) Also, compounds with MA, FA and G cations are efficient options for novel HIOP. Also, a mixed occupation in the site was investigated in the compound $MA_{1-x}G_xPbI_3$, which has better stability after the incorporation of a large G cation than pure $MAPbI_3$, in addition to an average PCE over 19%. Such G/MA combination implies better photovoltaic performance and good optoelectronic properties associated with the organic lead halide materials. (JODLOWSKI et al., 2017; VEGA; MOLLAR; MARÍ, 2018)

More recently, some investigations were focused on the combination of different anions in the HIOP. This combination can be an excellent solution for improved and better efficient materials, putting together those be characteristics of both elements. For example, the compounds $MAPbCl_xI_{3-x}$ and $MAPbBr_{3-x}Cl_x$, which have the same orthorhombic family than pure $MAPbX_3$ (X=Cl; Br and I), were investigated. This new class of semiconductors exhibit excellent performance as active layers in photovoltaic solar cells (ODENTHAL et al., 2017) and bring an unprecedented opportunity for radiation detection with their defect tolerance nature, high mobility-lifetime product, and simple crystal growth solution. (WEI et al., 2017) Interestingly, despite the apparent high quality of most of the single crystals investigated, there is a small variation in the optical properties (absorption and photoluminescence). There is currently an intense debate about what mechanism drives the second-order electron-hole recombination. (HUTTER et al., 2016) Also, DMA was incorporated in simple perovskite $CsPbI_3$, forming $Cs_{0.7}DMA_{0.3}PbI_3$, the whose based solar cell absorbs yielded much better than the simple one. (KE et al., 2018)

Particularly, in the case of DMA anion, it was reported that in compounds with this ion, they are highly responsible for ordering in the crystal structure at low temperatures, and most cases responsible for the ferroelectric order. (JAIN et al., 2008) One compound that presents an interesting ferroelectric ordering transition at low temperatures is the metal composition $DMAZn(HCOO)_3$. This compound was characterized by single-crystal X-ray diffraction at low temperature, and DSC, which determined a structural phase transition at 156 K. Such transition is an order-disorder type, and dielectric constant measurements showed that at this transition it happens an electrical ordering implying in ferroelectric properties.

As was described, the amount of organic cation incorporated in the perovskite structure has a huge effect on the material properties. Also, dimethylammonium can experience thermally induced order-disorder processes in hybrid perovskites, inducing structural phase transitions with associated interesting properties, dielectric transitions and cooperative in the electric order. The ordering of DMA cations is associated with a decrease in symmetry in the crystal structure, but a detailed mechanism of the phenomena is still not fully understood. (BESARA et al., 2011) Even though, transitions associated with an order-disorder evolution are found in a wide semiconductor and glassy materials.

Chapter 2: Experimental and Theoretical Procedures

In this chapter, we present the experimental details employed along with the techniques used to investigate the $DMAPbBr_3$ and the $DMA_7Pb_4Br_{15}$ crystals. Besides, we shortly describe the phonon calculation method to assign DMA Raman-active phonons in the crystals.

2.1. Synthesis Procedures

All starting materials were from commercial sources, with the exception of $(CH_3)_2NH_2Br$ (DMABr). The compound $PbBr_2$ (99%), HBr solution (48 wt% in H_2O) and N-dimethylformamide (99%) $(CH_3)_2NCHO$ (DMF) were purchased from Sigma-Aldrich and Alfa Aesar.

$DMAPbBr_3$ crystals

The first step was the synthesis of the $(CH_3)_2NH_2Br$ (DMABr) (combination of the organic molecule and Br element), the dimethylamine $(CH_3)_2NH$ solution in a slight excess was reacted with hydrobromic acid (HBr) in an ice bath. The crystallization of dimethylammonium bromide $(CH_3)_2NH_2Br$ was achieved using a rotary evaporator; a white colored powder was formed indicating successful crystallization. The white microcrystals $(CH_3)_2NH_2Br$ were washed with absolute diethyl ether several times, and finally dried under vacuum overnight.

Single-crystals of $DMAPbBr_3$ has been obtained by crystallization from N, N-dimethylformamide (DMF) solution. For this purpose, stoichiometric amounts of $PbBr_2$ (4 mmol) and of DMABr (4 mmol) were dissolved by adding 5 ml of DMF. The obtained solutions were filtered through 0.45 μm PTFE filters to minimize nucleation sites. Colorless needle-shaped single crystals of $DMAPbBr_3$ were obtained upon slow evaporation of the solvent at room temperature after several days.

Additionally, powders of $DMAPbBr_3$ compounds were easily obtained at room temperature by the simple solid-state method of mechanosynthesis. For that, equimolar

amounts of $PbBr_2$ and DMABr were placed in an agate mortar and carefully ground with a pestle along 30 minutes.

Such crystals were synthesized in the Departamento de Química Fundamental in the Universidad de Coruña by Prof. Manuel Andujar in collaboration with Professor Rosivaldo Silva, and Ariel Nonato from Universidade Federal do Maranhão.

$DMA_7Pb_4Br_{15}$ synthesis

The composition $DMA_7Pb_4Br_{15}$ was also synthesized by the slow evaporation method. The phase was mixed $PbBr_2$ and DMABr with a stoichiometric ratio 1:1 in a bottom of the flask containing 3mL of DMF precursor. The mixture was placed under stirring and heating at 100 °C for 1h. After that, the solution stood for a 1 day until. The final product was filtered and washed with ice-cold ethyl ether and then stored under vacuum. The result was homogeneous single crystals and powdered examples of $DMA_7Pb_4Br_{15}$ crystals.

2.2. Structural Characterization

The Single crystal data were collected at different temperatures (300 and 150 K) in a Bruker D8 Venture X-ray diffractometer equipped with a Photon II Kappa detector and using Mo Kα radiation (λ=0.71073Å). The crystals were chosen and mounted on a MiTeGen MicroMount using immersion oil. Were cooled at different rates using a nitrogen gas cold stream from an Oxford Cryosystems cooler. The data were indexed using CELL_NOW 2008/4. The integration was performed using SAINT V8.38A included in the APEX2 suite of software. The structures were solved by direct methods using the SHELXT/2015 program and were refined by least-squares methods on SHELXL/2008. To refine the structures, anisotropic thermal factors were employed in the Pb and Br atoms and for the DMA cations isotropic thermal factors.

2.3. Raman spectroscopy

As was described, the Raman spectroscopy is a susceptible technique to local symmetries; for these reasons, a good interpretation of results could be a powerful tool for the investigation in order-disorder crystals transitions. Thus, in order to investigate

any structural modification, the Raman analysis under temperature was performed in both small single crystals. The Raman-active spectra of the compounds were collected in a high-resolution LabRam HR Horiba 800 spectrometer using a grating with 1800 lines per millimeter and equipped with a CCD detector cooled with liquid nitrogen. In this equipment are available four optical sources for excitation: the 785 nm (infrared) line, the 488 nm (blue) and 514.5 nm (green) lines from an Ar^{+}-ion gas laser and the 632.5 nm (red) line from He-Ne gas laser. Was used the red laser as an excitation source, the beam was focused onto the sample using a long working distance 20x/0.40 microscope objective; the RTD exposure time was 1s, the exposure time 5s and the accumulation number was 20, the complete spectral range was 20-3200 cm^{-1}. Finally, the same experiment was done in the temperature variation from 300 K until 140 K, for this, the samples were placed in Nitrogen closed-cycle cryostat Linkam, whose temperature is controlled by a Linkam temperature software controller.

2.4. Differential Scanning Calorimetry

The thermal analysis was characterized by a differential scanning calorimetry technique; the analysis was performed on a Netzsch Maia 200 F3. Measurements were obtained from several cooling and heating cycles in different temperatures, the used rates were 5 $K.min^{-1}$ from 300K to 140K range, in this analysis were prepared two aluminum pans, the first one is for the sample and the second an empty for reference. For $DMAPbBr_3$ composition was deposited 7.0 mg of sample in a pierced aluminum pan, both the reference pan and prepare one were analyzed with the same past low-temperature treatment. Under a flow of dry nitrogen atmosphere were carried out the experiment, sensors and the crucibles were kept under a constant flow of nitrogen during the experiment. For $DMA_7Pb_4Br_{15}$ was deposited 5.0 mg of sample in a pierced aluminum pan and were used the same past process.

2.5. Computational Modeling

The organic part DMA cation as was described can experience thermally induced order-disorder processes in hybrid perovskites and in some cases structural phase transitions with associated interesting properties. For this reason, we performed a DFT calculation with DMA molecule in Gaussian09 software (FRISCH et al., 2009) to assign

its vibrational modes. For these calculations, was used the Opt+Freq in the job type window, also were used a tight convergence criteria, for optimize the molecule to a minimum and compute the Raman spectra, in the method window was used an ground state, DFT, unrestricted and B3LYP functional, with a 6-311G, ++ (d,p) base, a charge equal 0 and singlet spin.

Chapter 3: The structural phase crystal transition on hybrid organic-inorganic halide like-perovskite $DMAPbBr_3$

Introduction

Actually, multiples hybrid inorganic-organic perovskites (HIOP) have been reported for the remarkable properties and there significant success in the applications as solar cells, light-emitting diodes, and photodetectors; in this compounds the organic cation constitutes in the structure an important feature for high-efficiency formulations, such as the long diffusion length, the largely tunable bandgap, and the high absorption coefficients, qualifying the perovskite as outstanding material for a variety of technological applications (WENGER et al., 2017b). For example, the insertion of dimethylammonium $[(CH_3)_2NH_2]^+$ (DMA) as organic cations on HIOP is interesting because, besides the photovoltaic and electronic properties, can be incorporated into different simple perovskites improving new results. (KE et al., 2018) Also, the compounds with DMA as anion has order-disorder type transition at low-temperature because this molecule is highly responsible for ordering in the crystal structure and most cases responsible for the ferroelectric order (ALBERTO GARCÍA-FERNÁNDEZ et al., 2018; JAIN et al., 2008). Some hybrid materials with DMA as cation and the chemical formula ABX_3 are the like-perovskites $DMAPbI_3$ (GARCÍA-FERNÁNDEZ et al., 2017) and $DMAPbBr_3$ (MANCINI et al., 2016).

The $DMAPbI_3$ is a 2H-hexagonal perovskite-like structure at room temperature belonging to the space group $P6_3/mmc$. This compound shows a direct optical band gap (E_g) of 2.39 eV, which is not suitable for photovoltaic applications. It undergoes an order-disorder first-order phase transition around 250 K when the structure goes to a monoclinic system belonging to the $P2_1/c$ space group. The mechanism of this phase transition is a combination of an ordering process involving DMA cation and an off-center Pb^{2+} cation shift. (GARCÍA-FERNÁNDEZ et al., 2017; JU et al., 2017; PEI et al., 2019) These results showed that DMA when replaces MA ion in $MAPbI_3$ (LEGUY et al., 2016) induced different structure and properties, as was discussed before.

By the other hand, few researches on the $DMAPbBr_3$ were performed. The investigations confirmed that, at room temperature, $DMAPbBr_3$ crystallizes into the hexagonal structure that belongs to the space group $P6_3/mmc$ (GESELLE; FUESS, 1997) the same space group than $DMAPbI_3$, including the DMA disorder. Another report, exhibit that the optical direct bandgap of the material is 3.03 eV (MANCINI et al., 2016) thus not represent a good candidate for solar cell applications. However, no reports about low-temperature stability on this compound were achieved. In this context, the $DMAPbBr_3$ represents a good candidate for the description of the order-disorder mechanism, the low-temperature structural phase transition, and the hybrid perovskites materials because we expect that the material has the same properties that are iodide family like-perovskite. For this reason, in this chapter, we discuss such stability of the compound employing Single Crystal X-ray diffraction (SCXRD), Differential Scanning Calorimetry (DSC) and Raman spectroscopy, separated in room temperature characterization and the novel structural phase transition.

3.1. Room temperature characterization

The $DMAPbBr_3$ crystalline structure was first reported by Geselle and Fuess (GESELLE; FUESS, 1997), they determined the crystal structure by SCXRD and described that the composition exhibit a hexagonal system belonging to the space group $P6_3/mmc$. Later, Mancini et al. (MANCINI et al., 2016) confirmed this structure by powder X-Ray Diffraction measurements. After the synthesis of the compound, we measured by SCXRD the $DMAPbBr_3$ single crystal. Our measurements are in agreement with the previously reported structure. This material displays a hexagonal system with a = 8.6159 (5) Å, b= 8.6159 (5) Å, c = 14.6256 (12) Å, $\gamma = 120^{\circ}$ and space group of $P6_3/mmc$ with four molecules per unit cell. The main feature of this structure is that it shows infinite constitutional chains of face-sharing $[PbBr_6]^{4-}$ octahedra along the c axis. Each chain is formed by $[Pb_2Br_9]^{5-}$ units, which is formed by two octahedra bounded by a common face, connecting three bromide ions. The units are connected along the chain by an octahedron corner. Thus, in the unit cell, there are two units, which are stacked along the c axis, being the second displaced of ½ diagonal on (110) direction. The DMA cations are in two different positions, 1) in the cavities left by the chains forming a distorted molecule with hexagonal symmetry where a complete nitrogen (N) atom is in the center and shared 1/6 carbon (C) atom is in the vertex (Type 1) and 2) in the vertex of

$DMAPbBr_3$ crystal structure and in the middle of the edge where 1/3 of C and 1/6 N atoms are bounded in a not defined structure (Type 2). These two types of disorder can be explained because the organic molecule has a really low-symmetry construction and in both cases is located in high symmetry position. The figure 4 shows the determined crystal structure of $DMAPbBr_3$ with all past description.

Figure 4: Crystal structure representation of the perovskite $DMAPbBr_3$ at room temperature.

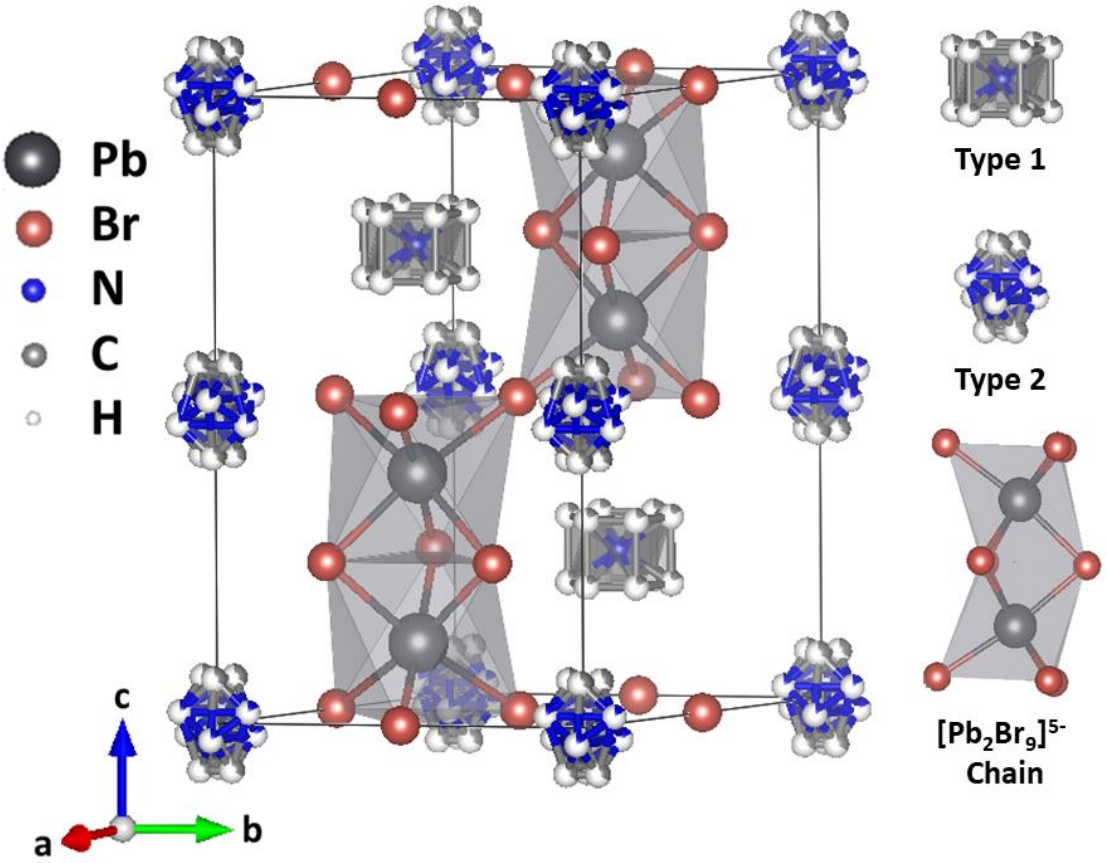

Observe that, besides $DMAPbBr_3$ and $DMAPbI_3$ exhibit the same symmetry at room temperature, the crystalline structures are quite different, as it is shown in Figure 5. While in $DMAPbI_3$ we have chains, in which the octahedral are only connected by the faces forming a two-dimensional perovskite, in $DMAPbBr_3$ there are the face and corner octahedra sharing along the chains forming a three-dimensional structure. However, the organic cation occupies only one site in $DMAPbI_3$, while in $DMAPbBr_3$ it occupies two different positions, in both cases the DMA organic molecule is distorted. For a clear view of the room temperature crystal structure $DMAPbBr_3$, we display it along with all directions in Figure 6. We can see in Figures 6 (a) and (b) how the $[PbBr_6]^{4-}$ octahedra

are linked to from the basic unit $[Pb_2Br_9]^{5-}$; while in Figure 6(c) is described the hexagonal base. These three visualizations highlight how DMA cation is disordered in both sites.

Figure 5: Comparison between the crystalline structures of $DMAPbBr_3$ and $DMAPbI_3$ at room temperature

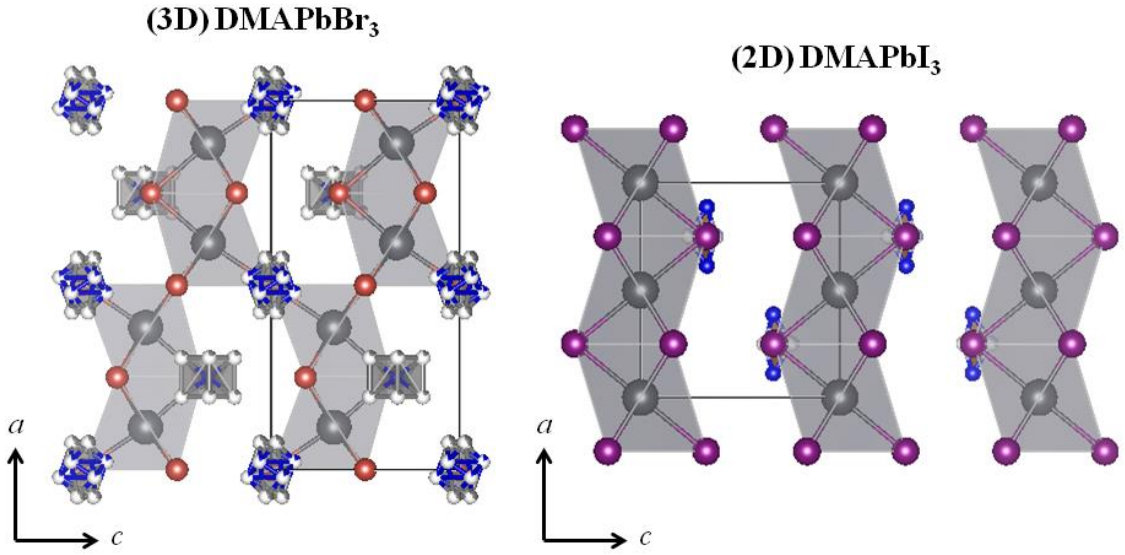

Figure 6: View of the crystal $DMAPbBr_3$ three-dimensional perovskite along the (a) a-axis, (b) b-axis and (c) c-axis at room temperature.

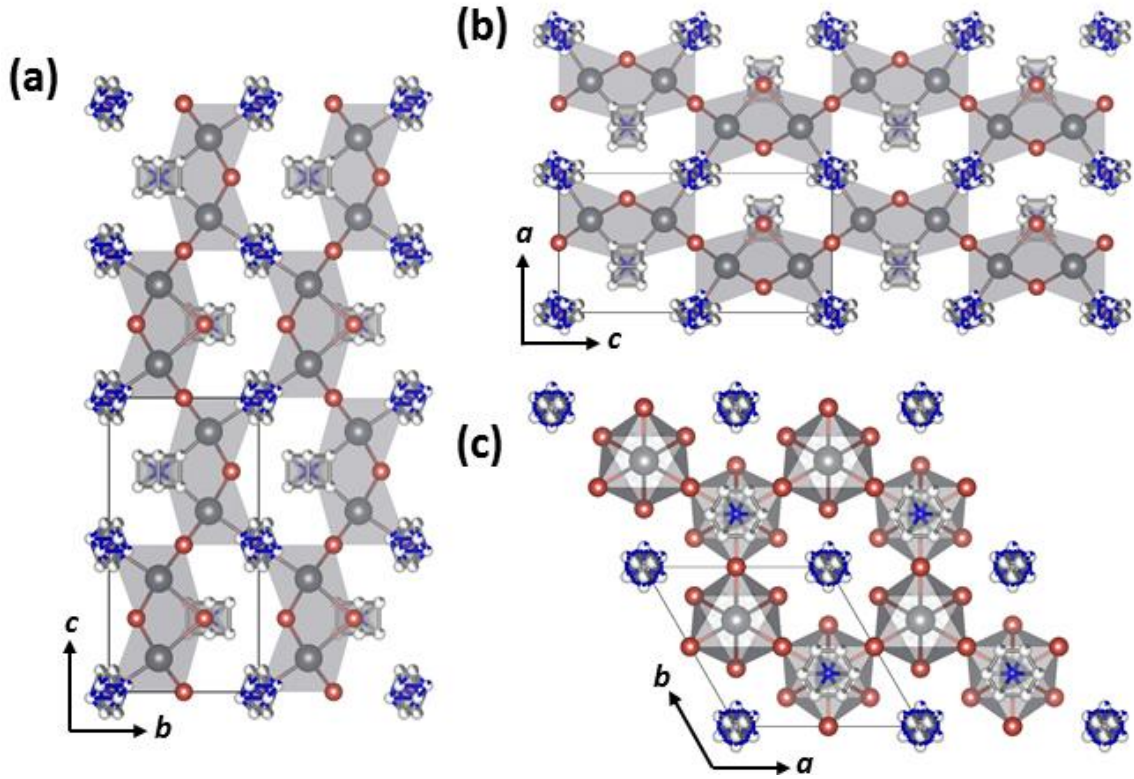

In this $DMAPbBr_3$, Pb cations are in a 4*f* wyckoff site whose symmetry is C_{3v}. There are two bromides, one in a 6*h* and other into a 6*g* wyckoff sites, the first one with symmetry 2/*m* (C_{2h}) and the other with symmetry *mm*2 (C_{2v}). The DMA cations are in two different crystalline sites and isotropically disordered in both places. Here, we consider the symmetry occupied by N to choice the symmetry occupied by all molecule because is the only element that is well defined. The first DMA (as whole) position is around the unit cell corners (See Figure 6(c)). In this position, N occupies a general symmetry site (1(*C*1) symmetry). In the second one, DMA is around the position (1/3; 2/3; 1/4) at the 2*c* site, with N occupying exactly this site, whose symmetry -6*m*2 (D_{3h}).

The Figure 7 shows the Raman spectrum of the crystal $DMAPbBr_3$ at room temperature. As we can see the Raman spectra are quite similar to others reported for hybrid perovskites with methylammonium cation $[CH_3NH_3]^+$ (MA) and Br, I and Cl halides anions. (LEGUY et al., 2016) Usually, the spectra of these compounds can be understood as consisting of two different parts: a low energy band of closely packed Raman peaks, commonly intense in range of 0-200 cm^{-1}, which are normally assigned as octahedra vibrational modes and organic cation translations; and the higher energy modes forming bands between 200 and 3200 cm^{-1} that are usually assigned to organic molecule. (LEGUY et al., 2016) For an easy interpretation of the Raman results, our spectra were separated in four different ranges: a) 20-300 cm^{-1}, b) 300-1100 cm^{-1}, c) 1200-1700 cm^{-1} and d) 2700-3200 cm^{-1}.

The fit with Lorentzians of our measured spectrum at room temperature is shown in Figure 8. We observed in all spectrum 27 Raman-active modes. As we discussed, DMA cation is disordered at room temperature. Thus, it is difficult to predict what is the symmetry of all modes at room temperature and defined the theory group in the material. All observed modes are shown in Table 1, which shows the comparison among the experimental modes, those calculated by DFT (See Appendix) and reported values for vibrations of the $[PbBr_6]^{4-}$ octahedra in different materials as $CsPbBr_3$, Cs_4PbBr_6, and $MAPbBr_3$.

Figure: Raman spectrum of the crystal $DMAPbBr_3$ at room temperature.

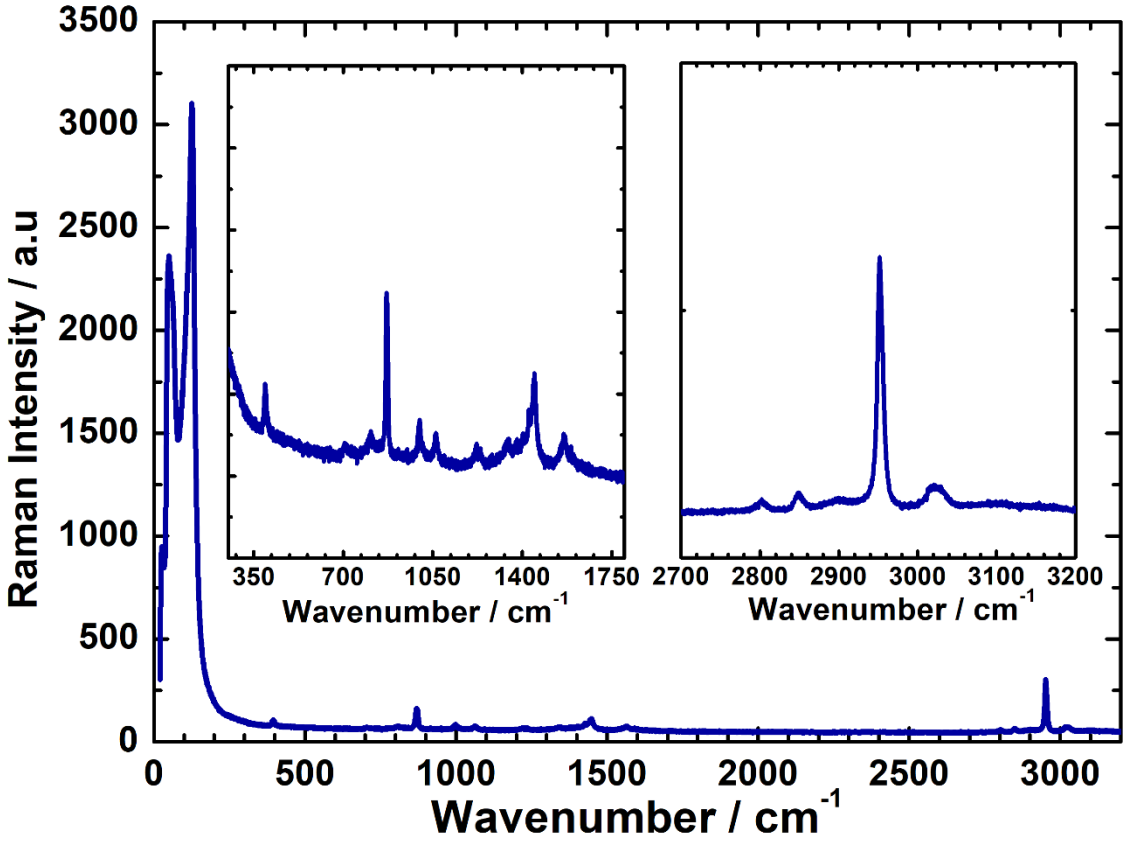

Figure: Raman spectrum fit as a convolution of Lorentzian functions of single-crystal $DMAPbBr_3$ at room temperature.

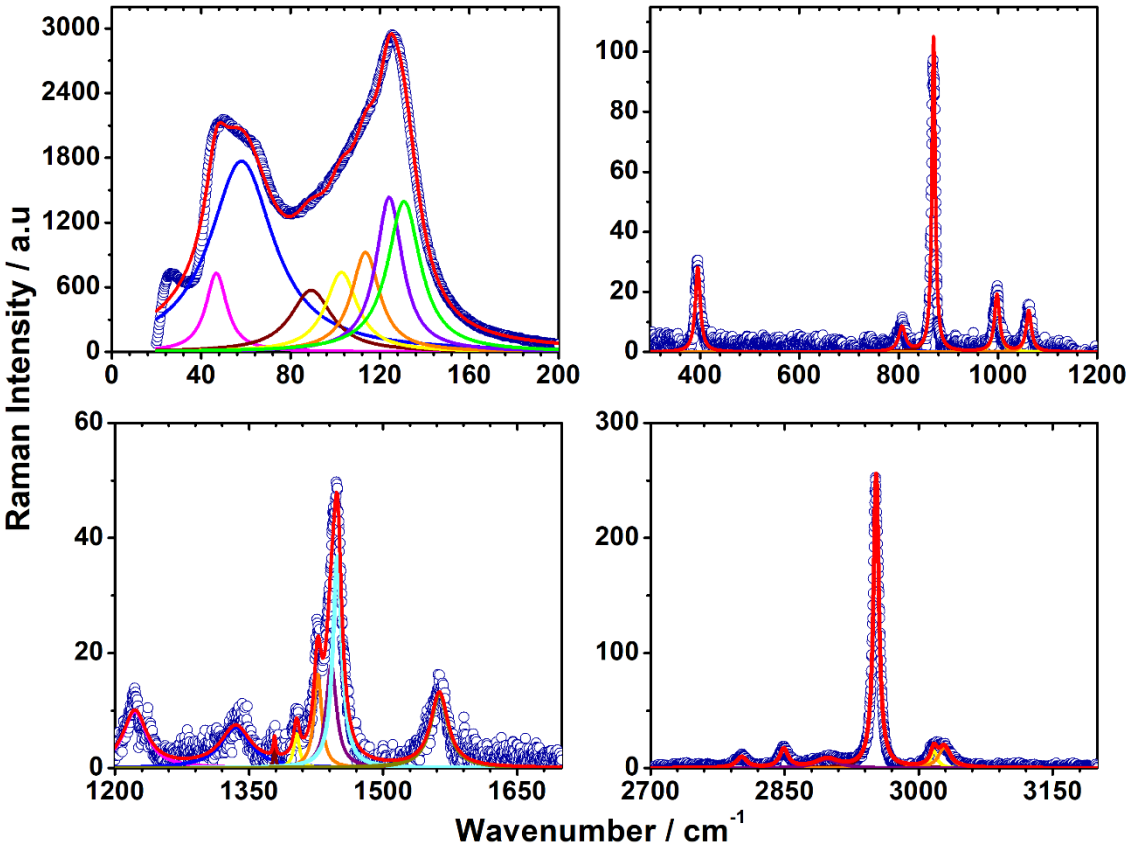

Table 1: Comparison among experimental, calculated and reported (for similar compounds) Raman-active modes in $DMAPbBr_3$ at room temperature.

Mode	Experimental (*f*)	DFT	Literature	Mode description
1	32		39 *	Octahedra Translation
2	50		47 *	Octahedra Translation
3	67		66 +	Octahedra Distortion
4	91		71 *, 72 +	Torsion in DMA (Type 1)
5	106		99 *	Torsion in Octahedra
6	113			Torsion in DMA (Type 2)
7	126		121 +,129 *	Torsion in DMA (Type 3)
8	146		138 *	Torsion in DMA (Type 3)
9	395		382 ^	$\omega(CH_3)$
10	807	771.0545		$\tau(CH_3)$; $\rho(NH_2)$
11	870	831.0575	820 ~	ν_s(C-N-C)
12	998		994 (MA) *	ν_{as}(C-N-C)
13	1062	1055.8152	1059 (MA) *	ν_{as}(C-N-C); $\omega(NH_2)$
14	1222	1230.6839		$\omega(CH_3)$
15	1335	1237.3043	1236 (MA) *	$\tau_s(CH_3)$; $\tau(NH_2)$
16	1378	1370.2386		$\omega_s(CH_3)$; $\omega(NH_2)$
17	1403	1402.0607		$\delta_s(NH_2)$
18	1427	1420.5244	1421 (MA) *	$\omega_{as}(CH_3)$; $\delta_s(NH_2)$
19	1442	1466.2218		τ_{as} (CH_3)
20	1449		1471 (MA) *	$\delta_{as}(NH_2)$
21	1563		1573 (MA)*	$\nu_s(NH_2)$
22	2802			$\nu_{as}(NH_2)$
23	2849		2821 (MA)*	$\nu_{as}(CH_3)$
24	2897	2876.6249	2896 (MA)*	$\nu_s(NH_2)$
25	2952		2965 (MA)*	$\nu_s(CH_3)$
26	3017			$\nu_{as}(CH_3)$
27	3029	3034.3830	3033 (MA)*	$\nu_{as}(NH_2)$

Abbreviations: DMA: Dimethylammonium; MA: Methylammonium; as: asymmetric; s: symmetric; ν: stretching; δ: in-plane bending; τ: twisting; ρ: rocking; ω: wagging. References: *:(LEGUY et al., 2016); +:(ZHANG; ZENG; WANG, 2017a); ~:(MA et al., 2018); ^: (TRIGUI et al., 2016).

The discrepancy on Table 1 may be due to an idealized comparison between a DFT calculation (Appendix) of the isolated DMA molecule cation and our single crystal. In addition, we associated two different organic compounds, for this reason, a range of 20 cm^{-1} was taken for the evaluation of these phonons. The Figure 9 shows how the octahedra with dimethylammonium could vibrate with a simple substitution of (MA) $[CH_3NH_3]^+$

for (DMA) $[(CH_3)_2NH_2]^+$ in the schematic representation of the vibrational modes geometries for $MAPbBr_3$. Even though the composition also has the same $[PbBr_6]^{-4}$ octahedra, they do not have the identical crystal structure, even the equal chain constitution, in this case the comparison of modes is not the best one. Nevertheless, a complete assignment of all room temperature Raman spectra was done, by the other hand, we still do not define the crystal phase transition of the hybrid perovskite with our room temperature characterization, or even, described if an order-disorder mechanism act, so in the following part we described these results.

Figure 5: Schematic representations of the vibrational modes geometries of the phonon modes of the methylammonium lead halides in the cubic phase for the octahedra composition. (LEGUY et al., 2016)

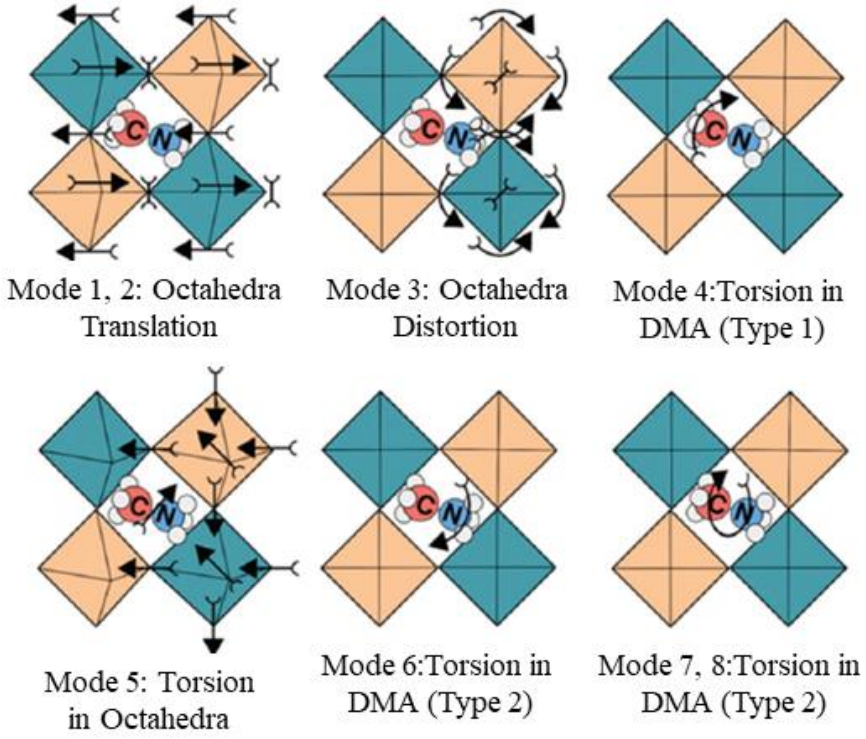

3.2. Structural Phase transition on $DMAPbBr_3$

To investigate the low-temperature stability in $DMAPbBr_3$ we performed DSC measurements. The DSC thermogram obtained for our sample is shown in Figure 10 between 150 and 300 K temperature range. We can clearly see a reversible first-order phase transition around 251 K (heating). Such transition exhibits a small thermal hysteresis, since during cooling the transition occurs at 250 K. The DSC behavior is very similar to others perovskites system contain DMA cation, as $DMAPbI_3$ (GARCÍA-

FERNÁNDEZ et al., 2017), $DMAZn(HCOO)_3$ (BESARA et al., 2011; ŠIMÉNAS et al., 2018, 2019) and DMA_7PbX_{15} (X= Cl or Br). (GARCÍA-FERNÁNDEZ et al., 2018) In all of these cases, the structural phase transition is associated with an order-disorder process of DMA cations. The main character in an order-disorder transition takes place from an ordered low- temperature to a disordered high-temperature phase.

Figure 6: DSC thermogram of heating and cooling cycles of the sample $DMAPbBr_3$ at $5K.min^{-1}$ between at 150-300 K range.

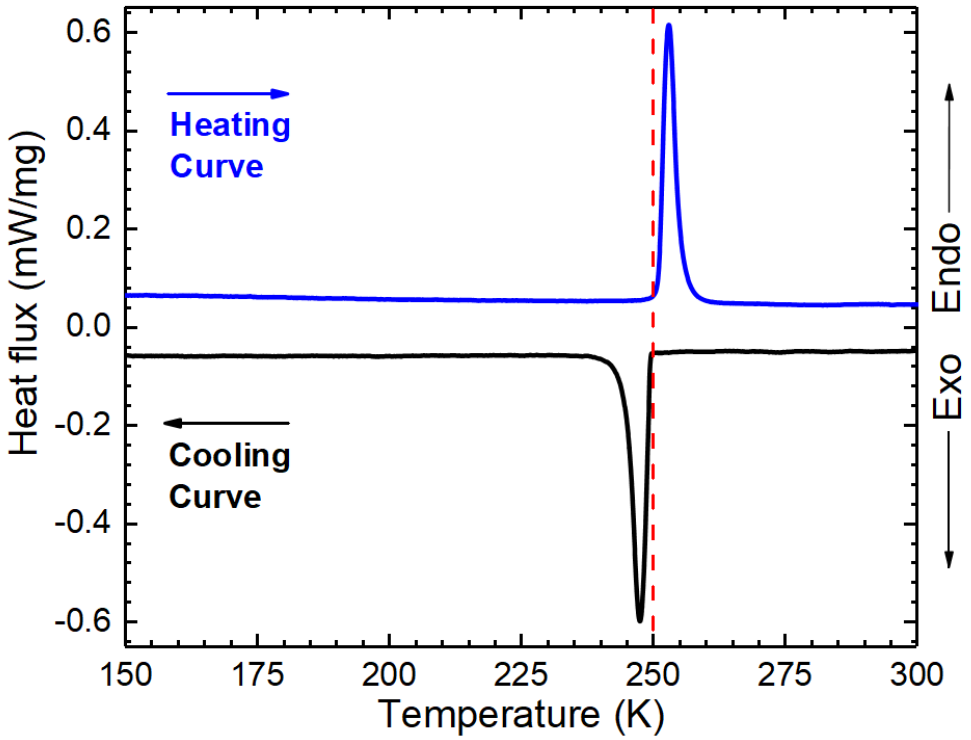

There is no indication of thermal hysteresis taking account the experimental precision. The peak area indicates an enthalpy variation of $\Delta H = 10.31\ Jg^{-1}$, which implies an entropy variation of $\Delta S = 20.33\ JK^{-1}mol^{-1}$. It suggests by these calculations at least 12 different disorder states for DMA organic molecule in the compound, this value is higher than reported in similar halide perovskites systems with DMA as a cation, such as $DMAPbI_3$ (GARCÍA-FERNÁNDEZ et al., 2017), $DMAZn(HCOO)_3$ (BESARA et al., 2011; ŠIMÉNAS et al., 2018, 2019) and DMA_7PbX_{15} (X= Cl or Br). (GARCÍA-FERNÁNDEZ et al., 2018) Observe that this reflect that in $DMAPbBr_3$ our DMA is more disordering in relation to $DMAPbI_3$ structure. To characterize the low-temperature phase of $DMAPbBr_3$, we performed single-crystal X-ray diffraction at 150 K. Our result showed that the new phase is orthorhombic with lattice parameters a = 8.835(1) Å, b = 14.217(2) Å, c = 14.701(2) Å, belonging to the space group of $P2_12_12_1$. A view of this structure is

shown in Figure 11. This is very interesting because $DMAPbI_3$, which is isomorphic to $DMAPbBr_3$ at room temperature, undergoes a phase transition to the same temperature, but it transforms into a monoclinic structure $P2_1/c$. This shows that the substitution of iodide by bromide, which has a lower ionic radius, induces a different route on the structural phase transition undergone in $DMAPbX_3$ materials. More interestingly, both $P2_12_12_1$ and $P2_1/c$ are subgroups of $P6_3/mmc$ space group. However, the lower symmetric group $P2_1/c$ is not a subgroup of the higher symmetric $P2_12_12_1$ one. This indicates that a possible phase transition on $DMAPbBr_3$ for still more low temperatures or should be reconstructive.

The orthorhombic phase exhibits the same basic unit $[Pb_2Br_9]^{-5}$ forming chains staked along the c axis, as can be seen in Figure 12. Observe that in this phase, DMA cations are well ordered. The main difference between both structures is the cavity, in which is DMA. While in the hexagonal phase it is regular, well symmetric, in the orthorhombic phase such cavity distorts, as can be seen in Figure 13. More interestingly, the cavities distorted along the direction in which DMA aligns, as it is shown by the pale orange arrows. Thus, DMA ordering is due to steric effects. On Table 2 we show a resume of the structural data for the $DMAPbBr_3$, including a measurement at 200 K.

Figure 7: Crystal structure representation of three-dimensional perovskite $DMAPbBr_3$ at 250K.

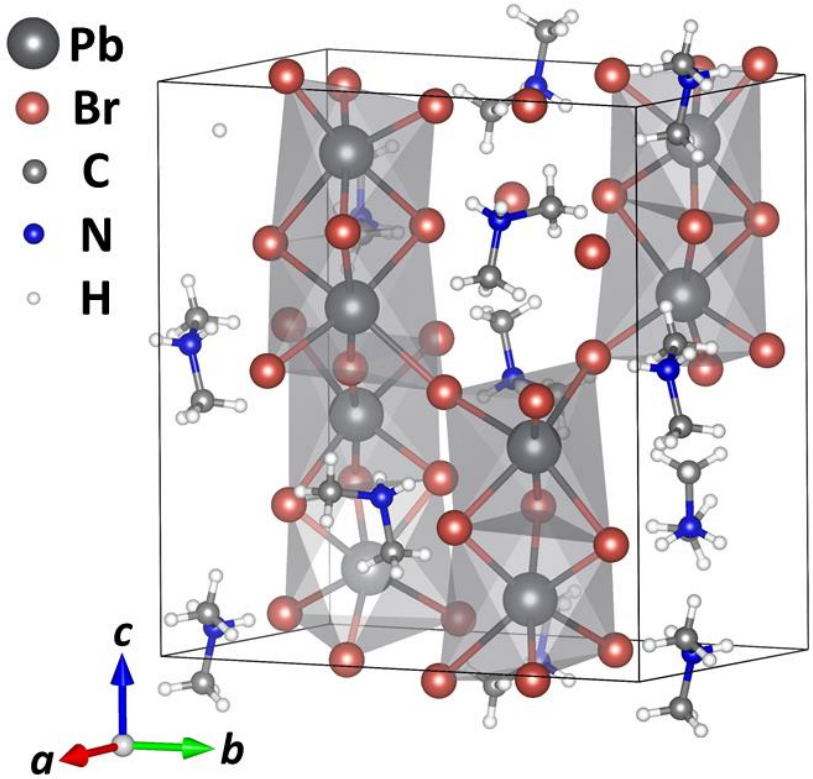

Figure 8: Different views of the crystalline structure of $DMAPbBr_3$ three-dimensional perovskite along the (a) *a*-axis, (b) *b*-axis and (c) *c*-axis at 250 K.

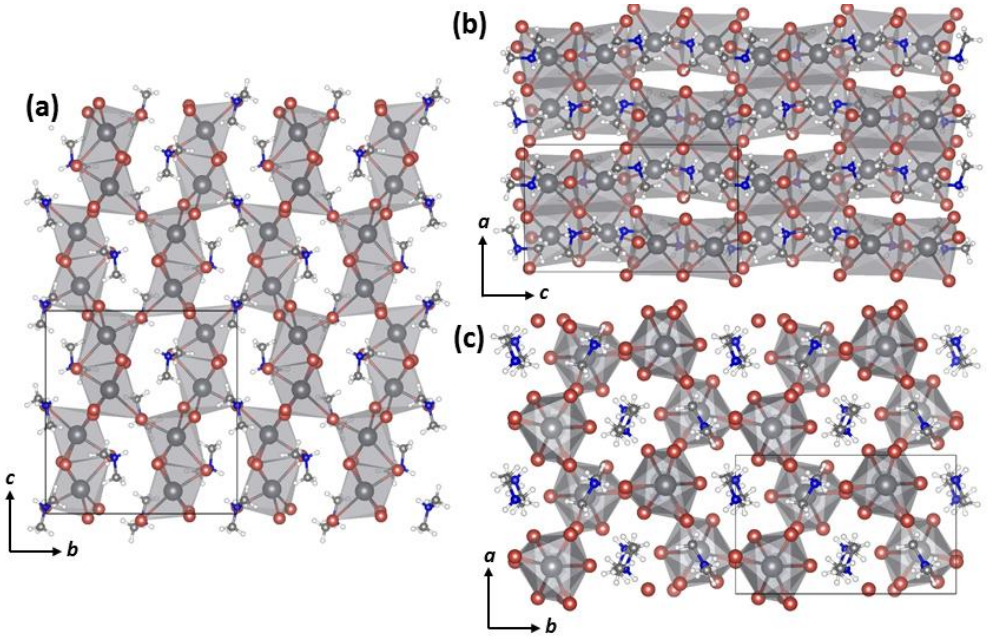

Figure 9: Comparison between the DMA cavities in both structures exhibited by $DMAPbBr_3$. Pale orange arrows show the direction in which the DMA cavities distort.

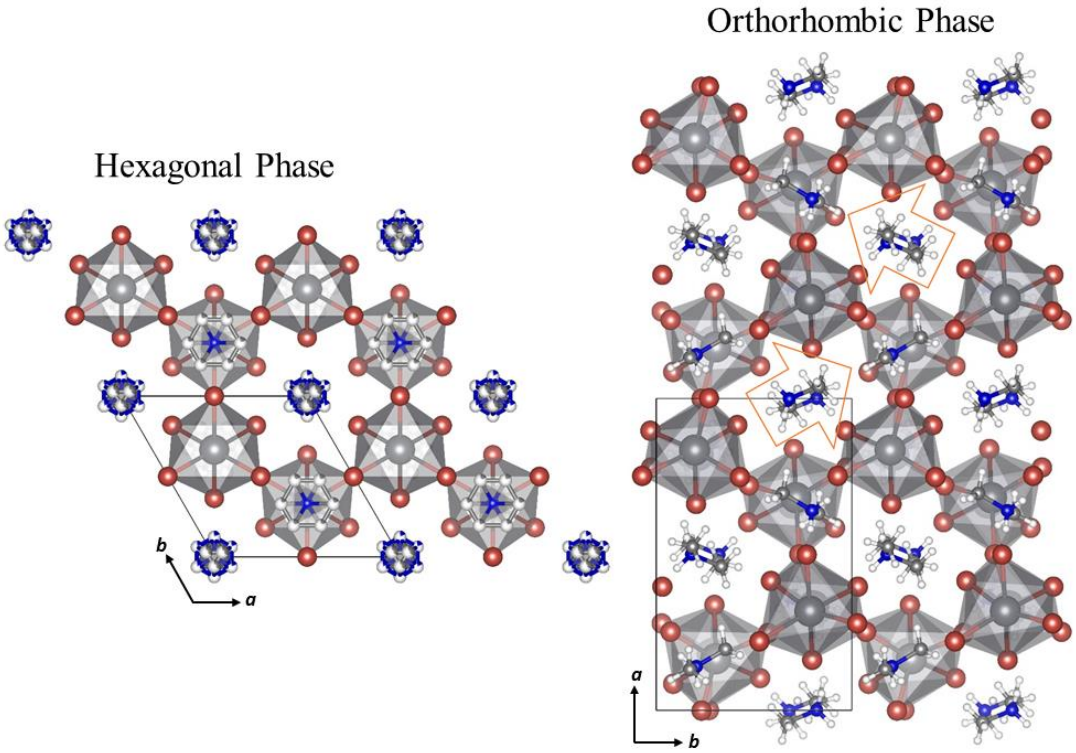

Table 2: Single-crystal X-ray data collection for $DMAPbBr_3$.

Empirical formula	$DMAPbBr_3$ * (293 K)	$DMAPbBr_3$ (302.3 K)	$DMAPbBr_3$ (249.9 K)	$DMAPbBr_3$ (200.0 K)	$DMAPbBr_3$ (152.4 K)
Formula weight	493	493.04	493.01	493.01	493.01
Wavelength	0.71073 Å	0.71073 Å	0.71073 Å	0.71073 Å	0.71073 Å
Crystal system	Hexagonal	Hexagonal	Orthorhombic	Orthorhombic	Orthorhombic
Space group	$P6_3/mmc$	$P6_3/mmc$	$P2_12_12_1$	$P2_12_12_1$	$P2_12_12_1$
Unit cell dimensions	a= 8.602(1) Å b= 8.602(1) Å c= 14.601(2) Å γ=120 °	a= 8.600(7) Å b= 8.600(7) Å c= 14.624(1) Å γ=120 °	a= 8.835(1) Å b= 14.217(2) Å c= 14.701(2) Å	a= 8.812(1) Å b= 14.122(2) Å c= 14.727(2) Å	a= 8.789(1) Å b= 14.042(3) Å c= 14.721(2) Å
Volume	935.6 $Å^3$	936.8(17) $Å^3$	1846.5(4) $Å^3$	1832.7(4) $Å^3$	1816.8(5) $Å^3$
Z	4	4	8	8	8
Density	-	3.496 mg/m^3	3.547 mg/m^3	3.574 mg/m^3	3.605 Mg/m^3
Absorption coefficient	307.6 cm^{-1}	30.721 mm^{-1}	31.171 mm^{-1}	31.406 mm^{-1}	31.682 mm^{-1}
F(000)	283	856	1712	1712	1712
Crystal size	0.21 x 0.23 x 0.4 mm^3	0.09 x 0.08 x 0.05 mm^3	0.11 x 0.08 x 0.06 mm^3	0.12 x 0.08 x 0.08 mm^3	0.11x 0.10x 0.09 mm^3

References: *:(GESELLE; FUESS, 1997)

To investigate phase transition on process DMA cation in low-temperature, we investigated the temperature-dependent Raman spectra of $DMAPbBr_3$, which is shown in Figure 14. At a glance, few changes happen in the Raman spectra. First, as is expected, there is a better definition of the modes for low temperature due to the reduction of the thermal analysis. Though, a more detailed analysis, we can see a low intense mode at 30 cm^{-1} is an indication of the phase transition. In fact, this model is near the detection limit of our spectrometer, and need to be confirmed. However, it looks like a soft mode, which confirms that the phase transition is not only due to the order-disorder process. For instance, other observations show the phase transition. Among them, we can cite: a change in the profile of the bands around 100 cm^{-1} and 111 cm^{-1} ; a shift in the band at 126 cm^{-1}; the low-temperature arising of the mode at 387 cm^{-1}, a shift in the modes at 395 cm^{-1} and 800 cm^{-1} modes, a peak profile change at 870 cm^{-1} around 140 K, the appreciation of a new crest in 1200 cm^{-1}, 1380 cm^{-1} and 1400 cm^{-1} and finally a peak profile modification in 2800 cm^{-1} and 2850 cm^{-1}. Figure 15 shows the temperature dependence

of the position of selected modes. As DMA turns ordered in the orthorhombic phase, we also expect that DMA modes suffer changes in FWHM parameter, since this parameter is related to the phonon lifetime, which is usually increased when ordering process occurs. The temperature dependence of this parameter for several DMA phonons is shown in Figure 16. As we can see, several modes have an abrupt decreasing in FWHM at the phase transition, which confirms the order-disorder nature of the phase transition.

Figure 10: Normalized Raman spectra separated in a) (0-600) cm^{-1}, b) (600-1800) cm^{-1} and c) (2700-3200) cm^{-1} regions for the range between 140 K and room temperature. The blue lines are the hexagonal phase and the green one the orthorhombic phase of single-crystal $DMAPbBr_3$.

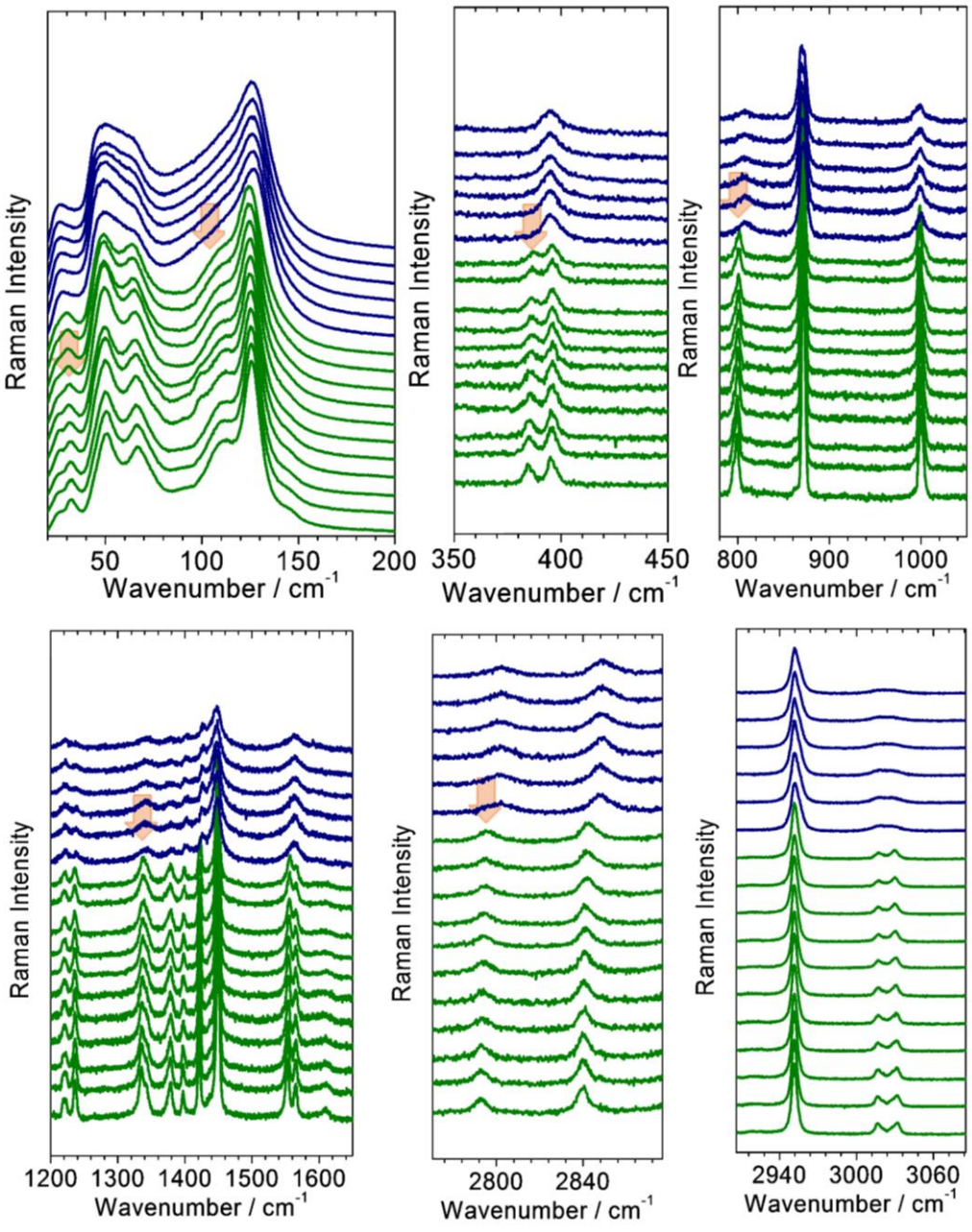

Figure 11: Temperature dependence of the phonon positions in $DMAPbBr_3$.

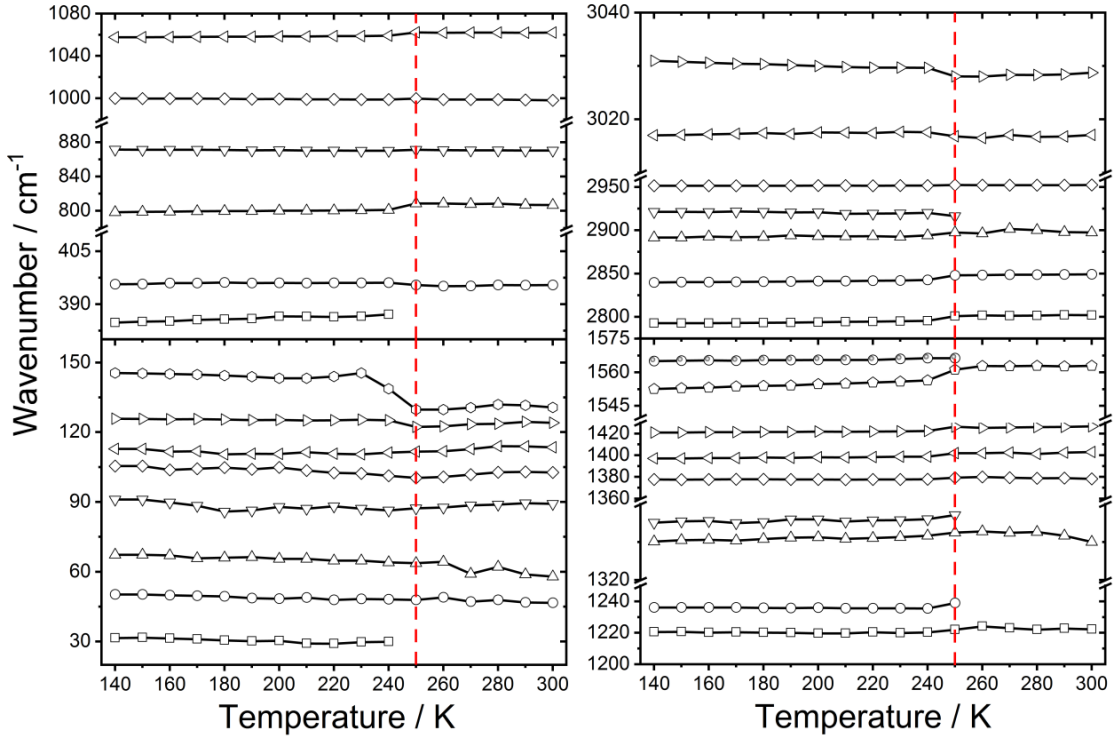

Figure 12: FWHM evolution in temperature of some phonon related to a phase crystal transition of single-crystal $DMAPbBr_3$.

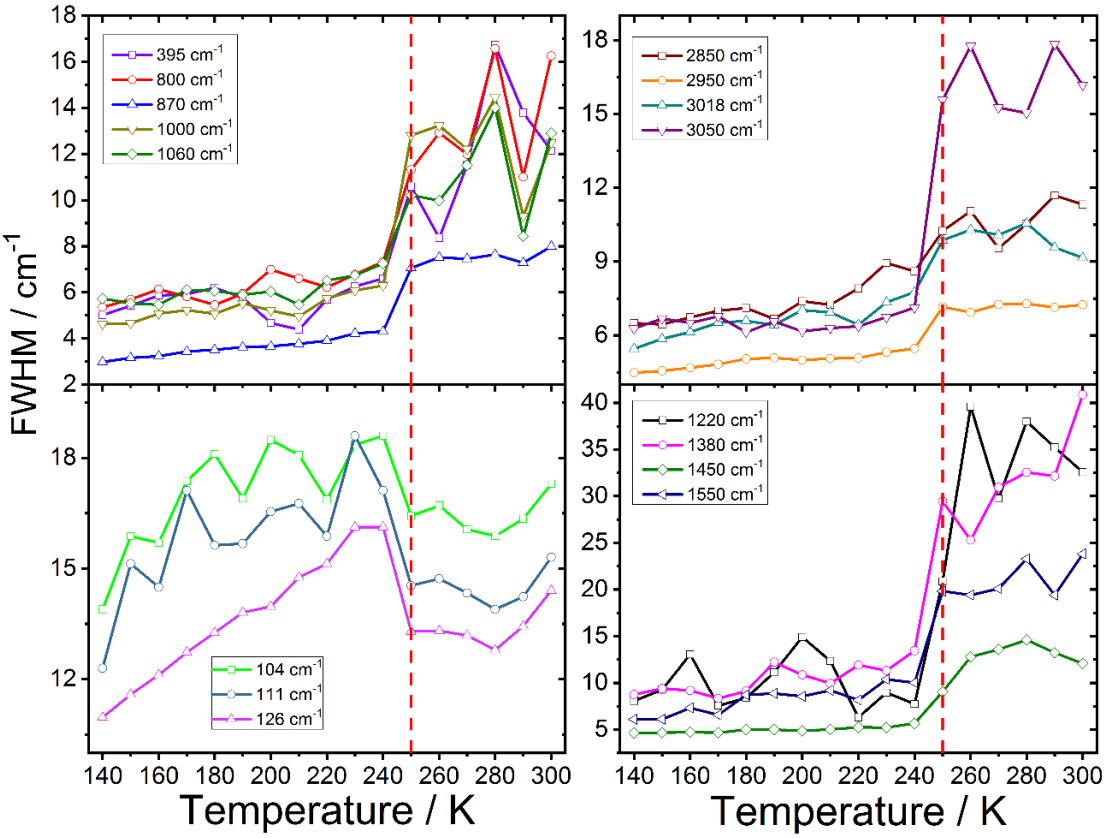

These results have some impact on the description of the properties and mechanism of the phase order-disorder phase transition. Also, describe a novel phase crystal

transition in a hybrid compound with possible, hoping applications. Furthermore, significant analyses could be carried on in this compound because has many advantages as an easy synthesized method and cheap materials and low-temperature formation.

Chapter 4: Study of the phase transition by Raman spectroscopy in the $DMA_7Pb_4Br_{15}$ perovskite

Introduction

As was described in Chapter 1, a simple way for understanding the perovskites crystal variations is classifying in the spatial arrangement of octahedral metal halide unit (BX_6), by a three (3D), two (2D), one (1D) and zero (0D) dimensional arrays. (LIN et al., 2018) Even though the 3D composition has a significant impact today, at the same time, there are significant amounts of recent works focused on the 2D materials because of their exhibit unique physical and chemical properties are arising from the plane quantum confinement effect. (TSAI et al., 2016) One of the most used applications of these two-dimension compounds is their stability in ambient, substantial and extending to application domains and construction for thin films research, in another perspective, these compositions have characteristics as large exciton binding energies, high quantum yields, and other rich photophysics properties. For all past reason, these 2D materials compositions find themselves as promising candidates for next-generation energy-efficient optoelectronics. (LAN et al., 2019)

Are suggesting that new halide inorganic-organic perovskites (HIOP) family with different stoichiometry and organic cation dimethylammonium $[(CH_3)_2NH_2]^+$ (DMA) could be synthesized, offering a novel possibilities in the hybrid perovskites world. In the 2D arrays, the DMF is used as co-solvent with chlorobenzene because helps the solubility and promote crystallization, (LETIAN DOU et al., 2015) the hybrid crystal structure $DMAPbI_3$ does not show a three-dimensional perovskites structure. Instead, crystallizes in a 2H-hexagonal compound consisting of infinite chains of face-sharing $[PbI_6]$ octahedra separated by chains of DMA cations. (GARCÍA-FERNÁNDEZ et al., 2017) The same crystal ABX_3 approximation used in $DMAPbI_3$ was made with the bromide halide (Br); the results of this composition were discussed in Chapter 3. In this context, with a little variation in the slow evaporation method synthesized part we obtained the material $DMA_7Pb_4Br_{15}$.

This compound was first reported by Garcia *et al.* (GARCÍA-FERNÁNDEZ et al., 2018), who obtained powders and single crystals compositions. This material has a block single-crystal form; it is colorless and does not degrade under room conditions for several months. They showed that at room temperature the perovskite crystallizes in a monoclinic system structure with a=17.086(3) Å, b=19.636(3) Å, c=16.431(3) Å, and β=105.719(1), belonging to $P2_1/c$ space group. As it is shown in Figure 17, the crystal structure is a two-dimensional single-layered lead halide framework with a DMA cation. This material exhibits a peculiar arrangement layer chains forming by Pb^{+2} cations with octahedral coordination and $[PbBr_6]^{4-}$ composition. In addition, at room temperature, the DMA cation is disordered in all $DMA_7Pb_4Br_{15}$ crystal structure, in a less proportion than the $DMAPbBr_3$ bromide halide compound discussed in the previous chapter.

Figure 13: Single-crystal structure of $DMA_7Pb_4Br_{15}$ perovskite at room temperature. This structure was designed using VESTA software. (MOMMA; IZUMI, 2011)

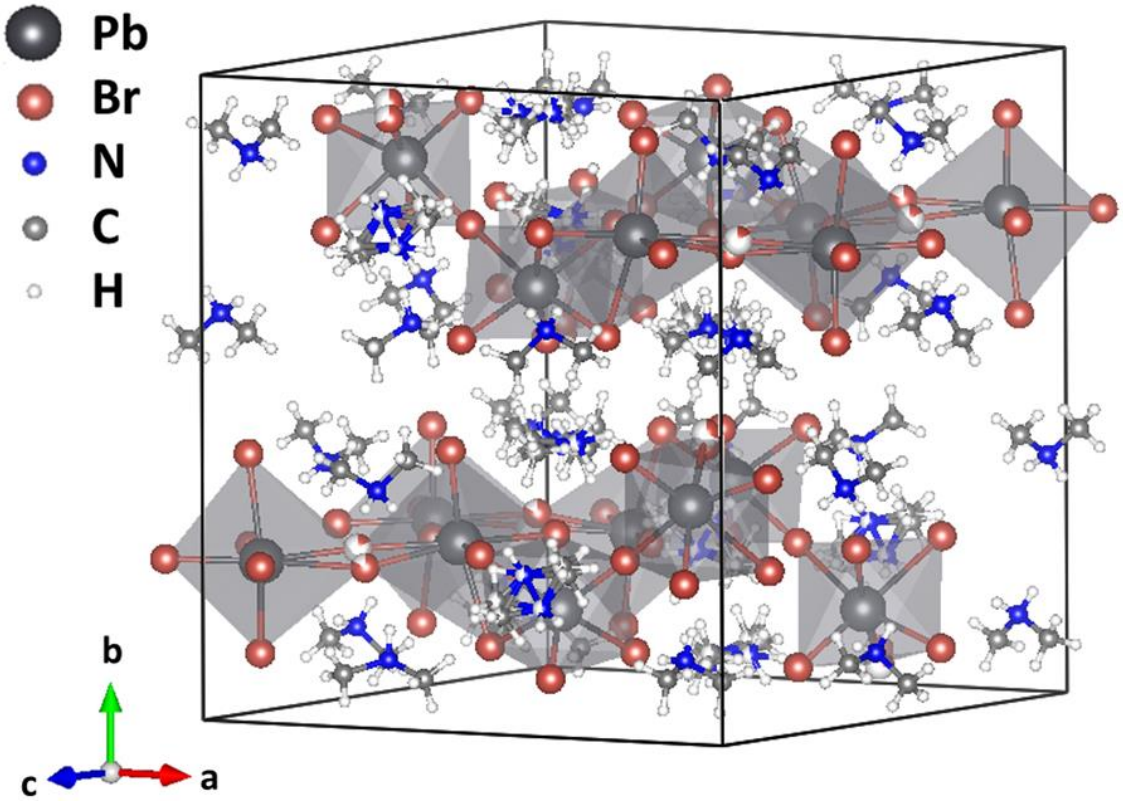

To describe a better chain constitution of the octahedral in the $DMA_7Pb_4Br_{15}$ material, in Figure 18 shows the (100), (010) and (001) plane views of the compound crystalline structure. First, we can see that the structure exhibit chains separated in the family plane (010), as it is shown in Figure 18 (a) and (b). Furthermore, Figure 18 (c)

shows that the four octahedra of the asymmetric unit are forming $[Pb_4Br_{15}]^{7-}$ chains, where two central $[PbBr_6]^{4-}$ octahedra are sharing one corner, and they are linked to the terminal $[PbBr_6]^{4-}$ octahedra by face-sharing. For an easy interpretation, it was removed the below plane and DMA cations in Figure 18 (c) to focus on the chain composes by $[PbBr_6]^{4-}$ octahedral. In addition, each $[Pb_4Br_{15}]^{7-}$ the chain is sharing corners with another $[Pb_4Br_{15}]^{7-}$ neighbor forming a 2D perovskite structured.

Figure 14: View of the crystal $DMA_7Pb_4Br_{15}$ along (a) the *a*-axis, (b) *c*-axis and (c) *b*-axis at room temperature. These structure views were designed using VESTA software. (MOMMA; IZUMI, 2011).

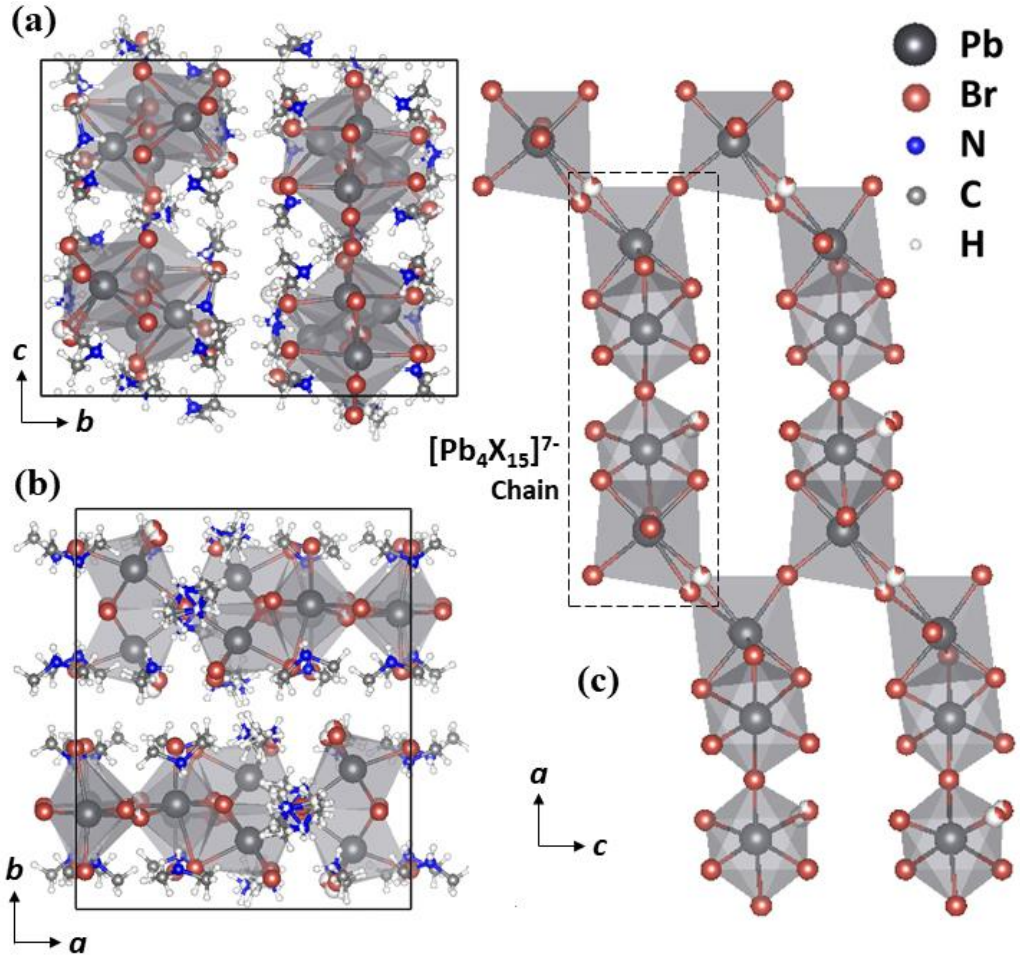

Also, Garcia *et al.* (GARCÍA-FERNÁNDEZ et al., 2018) showed that $DMA_7Pb_4Br_{15}$ undergoes a clear Structural Phase Transition (SPT) at 250 K, as well as exhibits two small thermal events at 182 K and 202 K, which were all determined by DSC. The Single Crystal diffraction measurements showed that this phase transition is isostructural at 100 K because the $DMA_7Pb_4Br_{15}$ presents the same crystalline structure than at room temperature. However, at low temperatures, DMA cation is ordered. In this

chapter, we present a Raman analysis of this SPT undergone by $DMA_7Pb_4Br_{15}$ since this technique is highly sensitive to the ordering in the material.

Results

As discussed in the experimental procedures, we obtained by slow evaporation synthesis method very small $DMA_7Pb_4Br_{15}$ colorless single crystals. To corroborate the crystal structure, for that, was carried at room temperature the Single Crystal X-Ray Diffraction (SCXRD) experiment. Our results confirmed the crystal structure of the perovskite composition, the compound $(DMA)_7Pb_4Br_{15}$ display a monoclinic system with *a*=17.0859(3) Å, *b*=19.6358(3) Å, *c*=16.4307(3) Å, β=105.719(1) ° and space group of $P2_1/c$. Our SCXRD collected data at room temperature shows good agreement with the structure determined by Garcia *et al.* (GARCÍA-FERNÁNDEZ et al., 2018). A comparison between both determined structures is given in Table 3.

Table 3: Reported crystal parameters for each lead hybrid halide perovskites.

Empirical formula	**$((DMA)_7Pb_4Br_{15})$** *	**$(DMA)_7Pb_4Br_{15}$**
Formula weight	2350.06	2104.48
Temperature	275(2) K	273(2) K
Wavelength	0.71073 Å	0.71073 Å
Crystal system	Monoclinic	Monoclinic
Space group	$P2_1/c$	$P2_1/c$
Unit cell dimensions	a=17.086(3) Å b=19.636(3) Å c=16.431(3) Å β=105.719(1) °	a=17.105(2) Å b=19.745(3) Å c=16.535(2) Å β=105.616(5) °
Volume	5306.3(16) $Å^3$	5378.3(12) $Å^3$
Z	4	4
Density	2.942 Mg/m^3	2.599 Mg/m^3
Absorption coefficient	23.967 mm^{-1}	23.627 mm^{-1}
$F_{(000)}$	4168	3568
Crystal size	0.24x0.06x0.02 mm^3	0.18x0.15x0.14 mm^3
Theta range for data collection	1.62 to 26.39	2.25 to 23.93

References: *:(GARCÍA-FERNÁNDEZ et al., 2018

Important structural characteristics of different HIOP compounds depend on external conditions, as temperature and hydrostatic pressure. For saw a better definition of dimethylammonium cation was done a low-temperature crystallographic structure determination to describe the possible structural order-disorder phase transition. In our low-temperature X-ray results, we described the crystal cell parameters variation in temperature. Figure 19 shows the temperature dependence of the lattice parameters of $DMA_7Pb_4Br_{15}$, in which the dashed red lines indicate the temperatures at which Garcia *et al.* (GARCÍA-FERNÁNDEZ et al., 2018) observed thermal events. We could see only slight changes in the lattice parameters. First, as expected, the lattice parameters *a*, *b*, and *c* decrease for low temperatures, as expected. Only *c* parameter exhibits clearer the phase transition at 250 K and the thermal event at 202 K. This behavior is reflected in the volume. While *a* parameter shows a subtle change in the inclination at 250 K, b parameter shows smalls fluctuations at 250 K and 200 K and 180 K. However, these changes in *a* and *b* are so small to be a guarantee that these parameters exhibit the SPT and the other two thermal events. This was expected since both thermal events are so weak and broad.

Figure 15: Temperature dependence of the lattice parameters *a*, *b*, *c*, V and β of $DMA_7Pb_4Br_{15}$. The dashed red lines indicate the temperatures at which Garcia et al. observed thermal events.

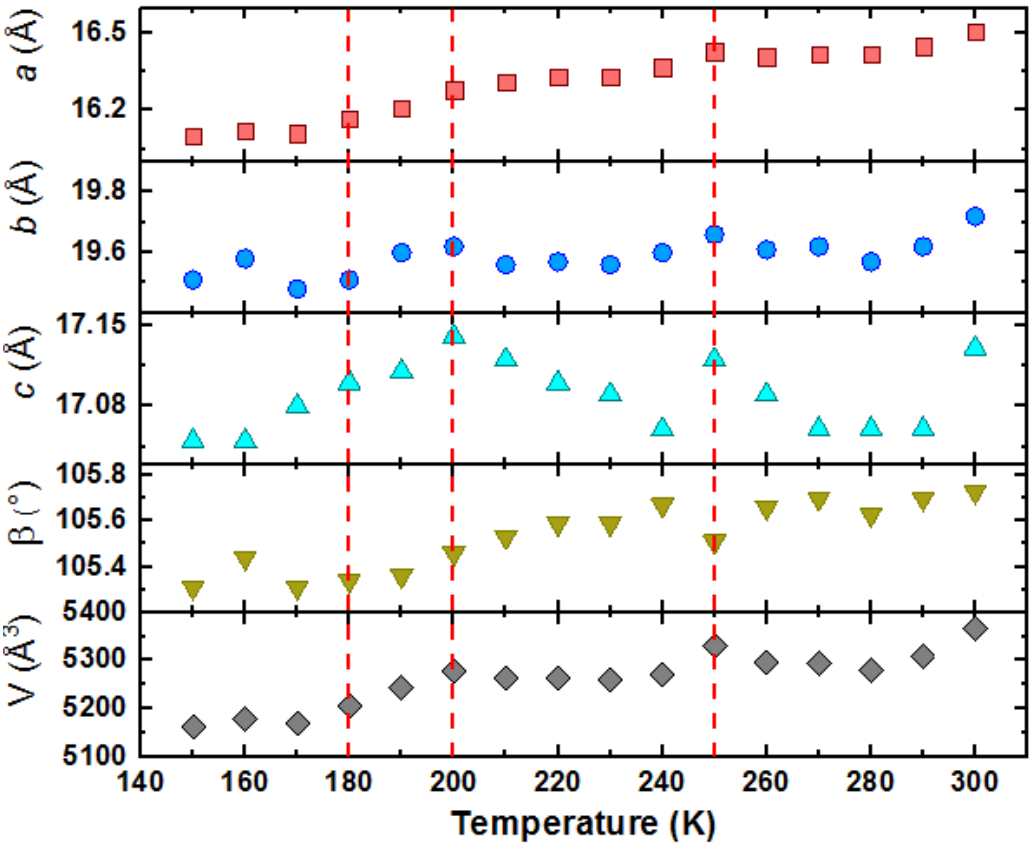

Even though this material has a defined crystal structure, are not reported yet the vibrational, rotational and frequency modes of the system, these analyses were described with our Raman spectroscopy. The Raman spectroscopy is a really susceptible technique to local symmetries; for these reasons, a good interpretation of results analysis could be a powerful tool for the investigation in order-disorder crystals transitions. Thus, in order to investigate any structural modification, the Raman analyses under temperature were performed in the same range stage that in the single crystal results. Figure 20 shows the Raman spectrum of $DMA_7Pb_4Br_{15}$ at room temperature. As we can see, this Raman spectrum is quite similar to that obtained for $DMAPbBr_3$ (Chapter 3), which is expected since $DMA_7Pb_4Br_{15}$ has the same $[PbBr_6]^{4-}$ octahedral and DMA cation, even though the organic DMA molecule does not have the same symmetry localization for that reason in these Raman spectra this part has more predominance.

Figure 16: Raman spectra of the crystal $DMA_7Pb_4Br_{15}$ at room temperature.

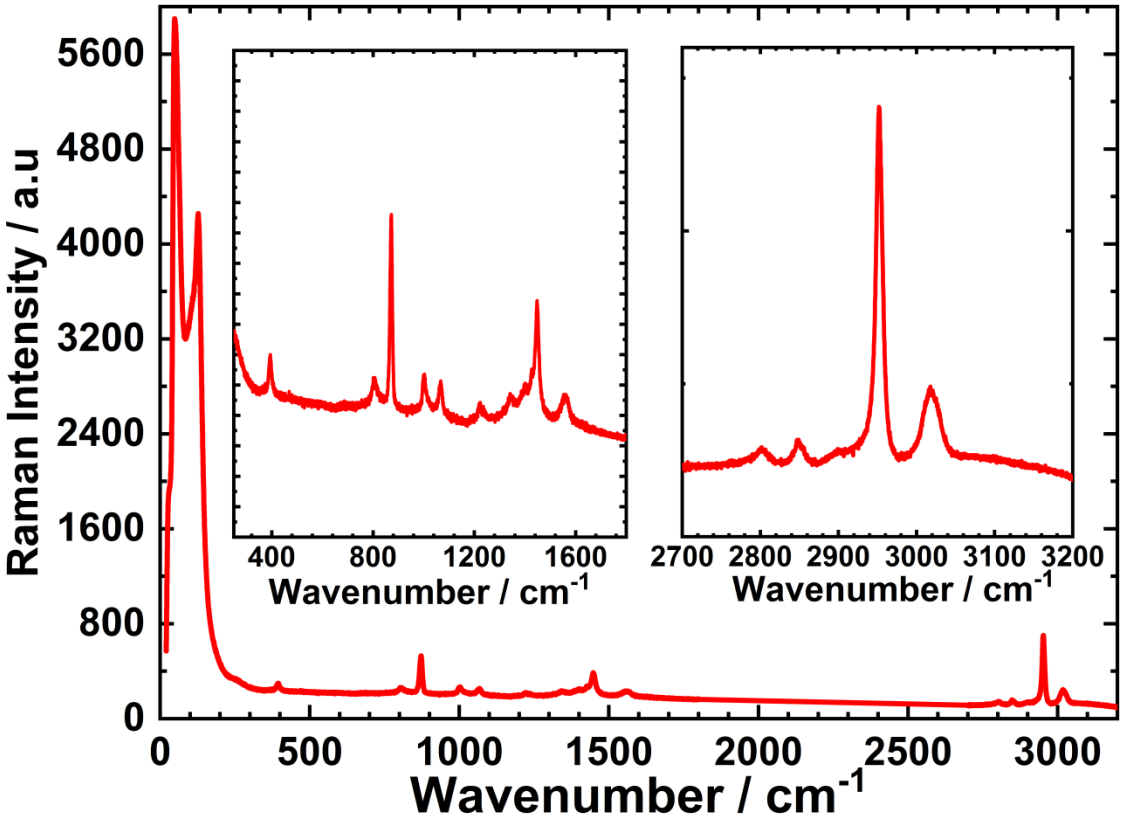

Actually, there are few reports on the literature showing the vibrational modes of hybrid perovskites, and usually, Raman investigations are normally separated in two different regions: i) low vibrations of the basic octahedral unit (frequencies up to 480 cm^{-1}) and ii) high frequencies for the organic part. For an easy interpretation of the Raman results, the spectra were separated in three different intervals, a) (0-250) cm^{-1}, b) (250-

1800) cm^{-1} and c) (2700-3200) cm^{-1} where each part was studied with a reliable fit of a convolution of Lorentzian functions, we described different vibrational characteristics for each peak characteristics, as the exact position in frequency of each crystal mode (maximum point of the peak), the phonon lifetime (FHWM) and intensity of the peak.

Figure 17: Raman spectra reliable fit of the Raman spectrum as a convolution of Lorentzian functions of single-crystal $DMA_7Pb_4Br_{15}$ at room temperature.

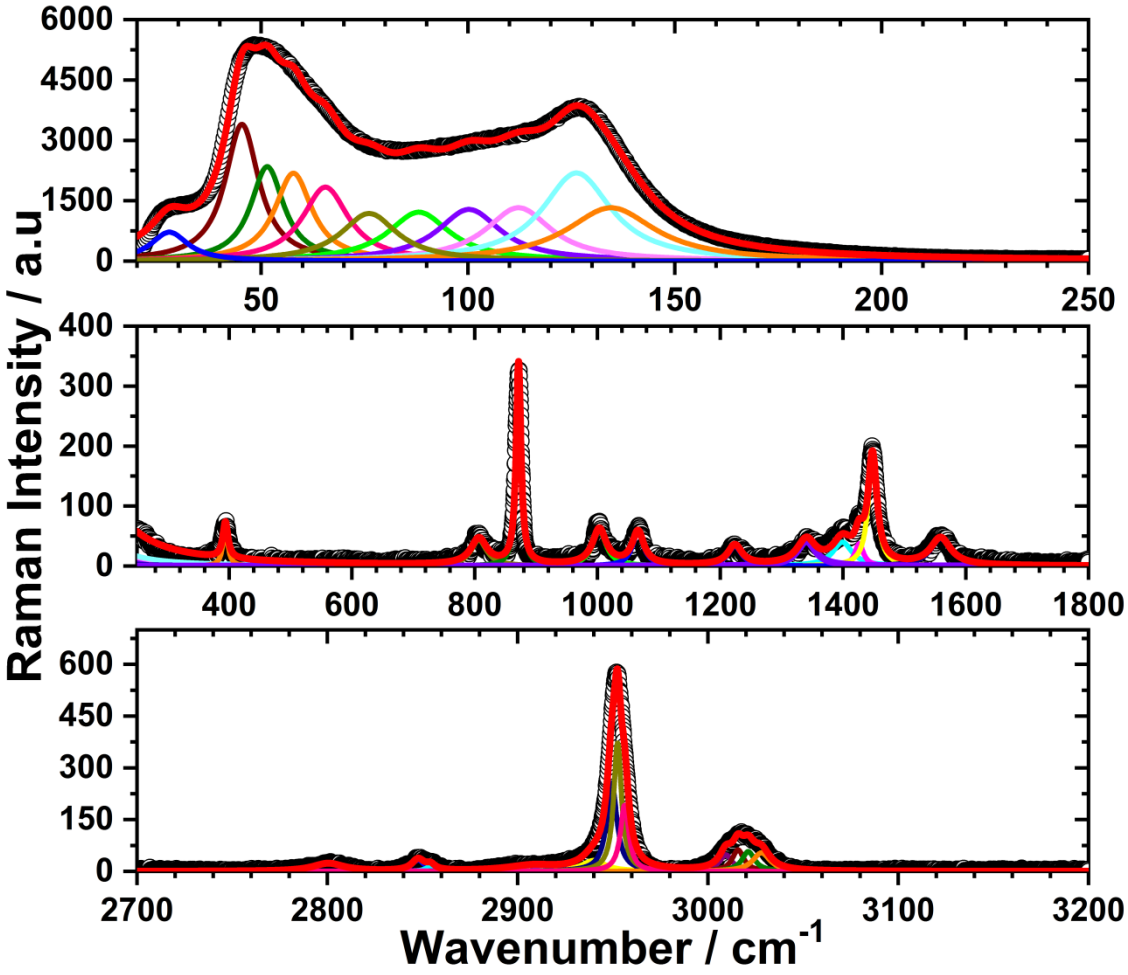

Each position of the peak for all deconvoluted Lorentzian function was compared with the literature, as was described; normally the vibrational modes of hybrid perovskites composition are separated in the vibration of the octahedra (low frequency) and an organic cation (high frequency). For the organic part was used as comparing the appendix A where is showed a DFT simulated Raman spectrum for dimethylammonium molecule and for the octahedral part reports about the $CsPbBr_3$, Cs_4PbBr_6, $MAPbBr_3$ at 100 K and our $DMAPbBr_3$ that are associated with the same $[PbBr_6]^{4-}$ octahedral. [9,11] All the assigned analysis is shown in Table 4.

Table 4: Vibrational frequencies comparison between the experimental values obtained with Raman spectroscopy, DFT calculations and reported frequencies (MA et al., 2018; ZHANG; ZENG; WANG, 2017b).

Mode	Experimental (*f*)	DFT	$DMAPbBr_3$	Literature	Mode description
1	27.80				Octahedra Translation
2	45.26			47 *	Octahedra Translation
3	51.45		50.32		Octahedra Translation
4	57.75				Octahedra Translation
5	65.48		67.38	66 +	Octahedra Distortion
6	75.95			71 *, 72 +	Torsion in DMA (Type 1)
7	87.96		91.20		Torsion in DMA (Type 1)
8	100.10		105.58	99 *	Torsion in Octahedra
9	112.09		112.89		Torsion in DMA (Type 2)
10	126.22		125.88	121 +,129 *	Torsion in DMA (Type 3)
11	134.51		145.55	138 *	Torsion in DMA (Type 3)
12	393.81	374.94	395.48	382 ^	$\omega(CH_3)$
13	806.74		806.83	820 ~	$\tau(CH_3)$; $\rho(NH_2)$
14	871.42	831.06	870.37		ν_s(C-N-C)
15	1003.06	1007.26			ν_{as}(C-N-C); $\omega(CH_3)$
16	1066.01	1055.82	1062.10	1059 (MA) *	ν_{as}(CNC); $\omega(NH_2)$
17	1223.81	1230.68	1222.36	1236 (MA) *	$\omega(CH_3)$
18	1340.26	1363.51	1335.16		$\tau(NH_2)$
19	1399.00	1402.06	1403.18	1421 (MA) *	$\delta_s(NH_2)$
20	1426.33	1420.52		1471 (MA) *	$\omega_{as}(CH_3)$; $\delta_s(NH_2)$
21	1447.98	1477.10	1448.94	1573 (MA)*	$\delta_s(CH_3)$
22	1558.95		1562.97	1552 ~	$\nu_s(NH_2)$
23	2800.51		2802.01		$\nu_s(NH_2)$
24	2847.70		2849.22		$\nu_s(NH_2)$
25	2854.25	2876.62		2871 ~	$\nu_s(NH_2)$
26	2907.81		2897.48		$\nu_s(CH_3)$
27	2940.09				$\nu_s(CH_3)$
28	2949.45				$\nu_s(CH_3)$
29	2952.50		2952.37		$\nu_s(CH_3)$
30	2956.18			2965 (MA)*	$\nu_s(CH_3)$
31	3009.38				$\nu_{as}(CH_3)$
32	3015.78		3017.10		$\nu_{as}(CH_3)$
33	3021.19				$\nu_{as}(NH_2)$
34	3028.08	3034.38	3028.78	3033 (MA)*	$\nu_{as}(NH_2)$

Abbreviations: DMA: Dimethylammonium; MA: Methylammonium; as: asymmetric; s: symmetric; ν: stretching; δ: in-plane bending; τ: twisting; ρ: rocking; ω: wagging. References: *:(LEGUY et al., 2016); +:(ZHANG; ZENG; WANG, 2017a); ~:(MA et al., 2018); ^: (TRIGUI et al., 2016).

Even though a complete assignment was done, we still do not define the crystal transitions of 2D hybrid perovskite, or even, described if an order-disorder mechanism act. For an investigation of the order-disorder DMA cation in low-temperature, we carried

out the variation of Raman spectrum. In Figure 22 are shown the normalized temperature-dependent Raman spectra of $DMA_7Pb_4Br_{15}$from 20 cm^{-1} to 3200 cm^{-1}, in the range from 150 K up to room temperature.

Figure 18: Normalized Raman spectra separated in a) (0-600) cm^{-1}, b) (600-1800) cm^{-1} and c) (2700-3200) cm^{-1} regions in different temperatures of single-crystal $DMA_7Pb_4Br_{15}$ for the range of 150 K until room temperature.

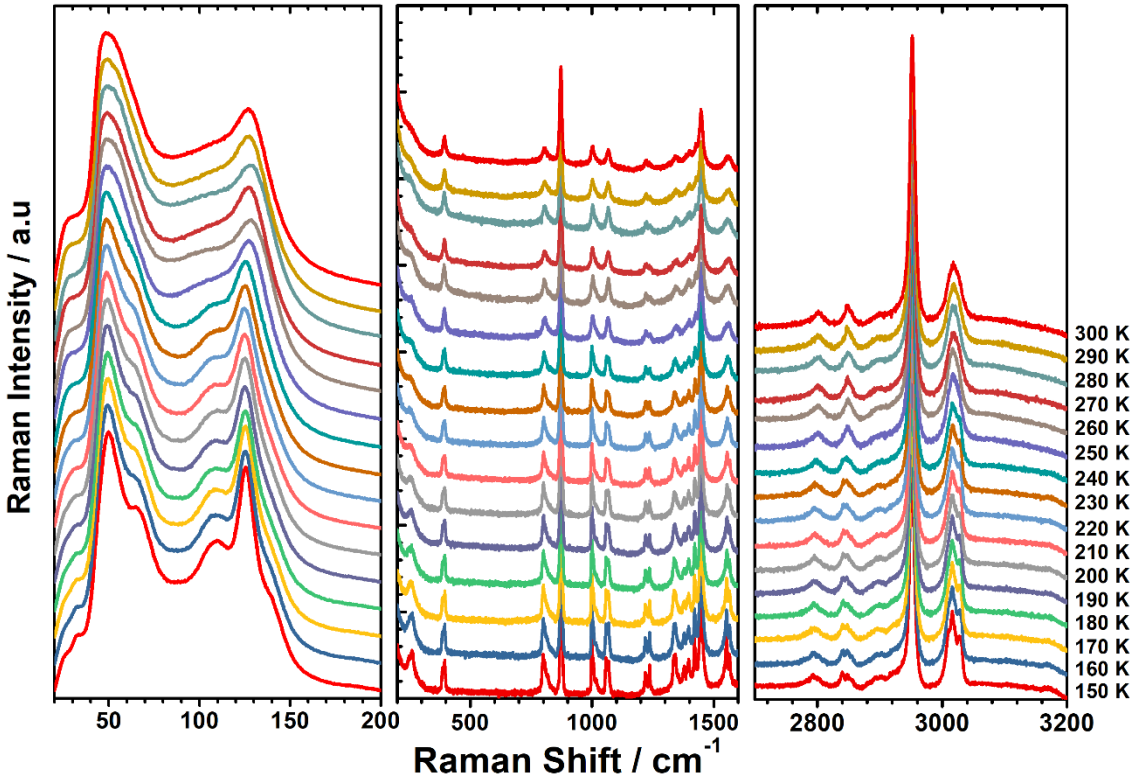

As we can see, any remarkable change happens in the spectra. This was expected since this SPT is isostructural. Even though, some crest appearance and alteration in relative intensity of the Raman peaks could define our phase transition. For instance, exits a clue to define an order-disorder transition in the material about 250 K designed for the presence of 60, 110 and 3100 cm^{-1} peaks because similar behavior present the crystal compound $[(C_3H_7)N]_3Bi_3Cl_{12}$ (TRIGUI et al., 2016), but the other phase transition (200 K) is not defined yet. For a better development of Raman under temperature results, just the high frequencies Raman spectra were fitted with a reliable adjustment of convolution of Lorentzian functions for each temperature, because fits over low-frequencies could do not described important changes for the isostructural crystal behavior, were defined the variation of the maximum point of the peak, the phonon lifetime, the area of the band and relative normalized intensity of the peak for a better phase transition definition.

Figure 19: Temperature dependence of the phonon positions in $DMA_7Pb_4Br_{15}$

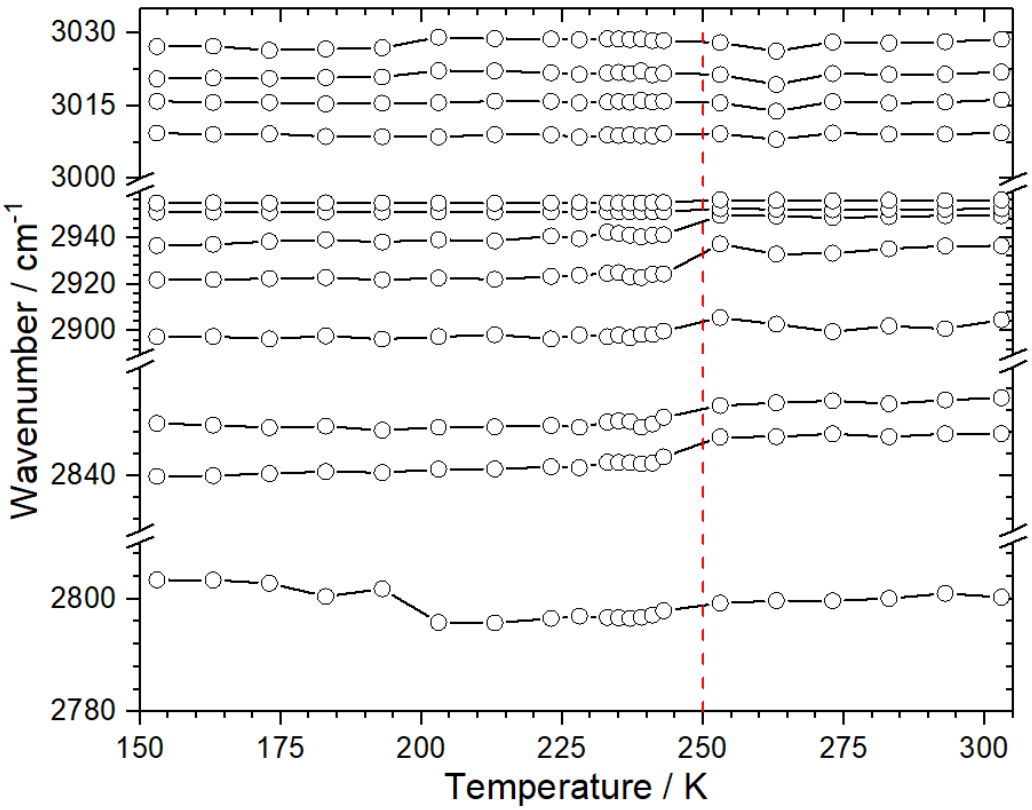

Figure 20: Temperature dependence of the FWHM of some vibrations in $DMA_7Pb_4Br_{15}$ crystal

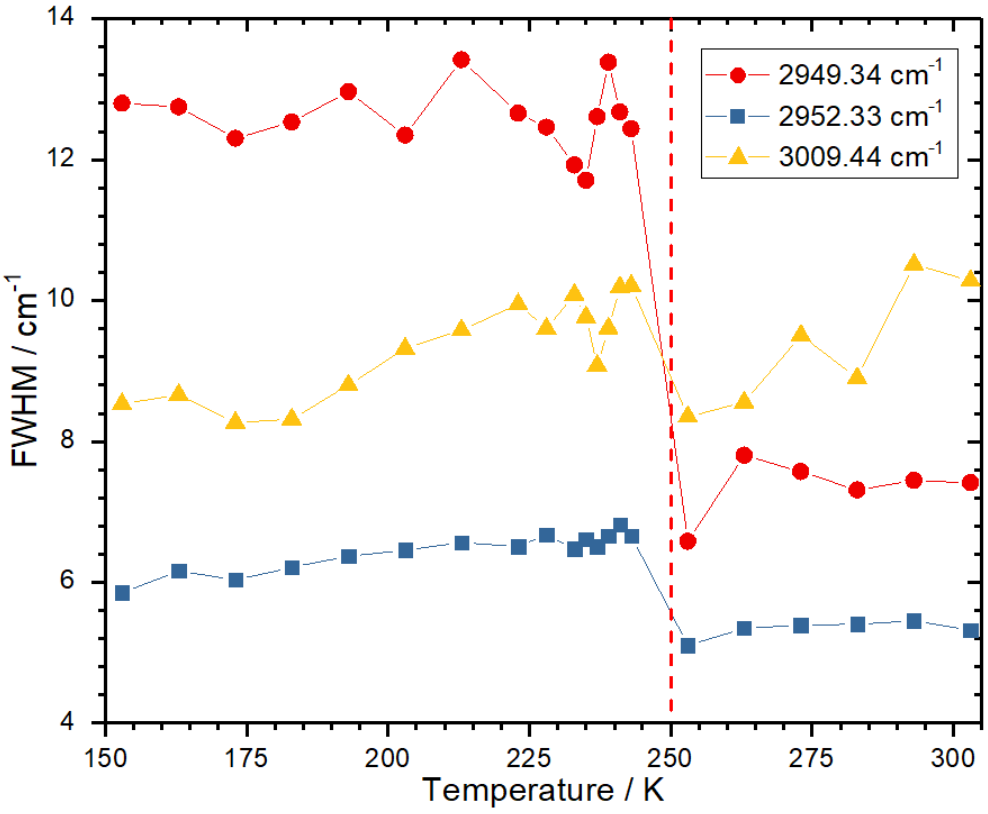

Figure 21: Temperature dependence of the area of the peak for some phonons in $DMA_7Pb_4Br_{15}$

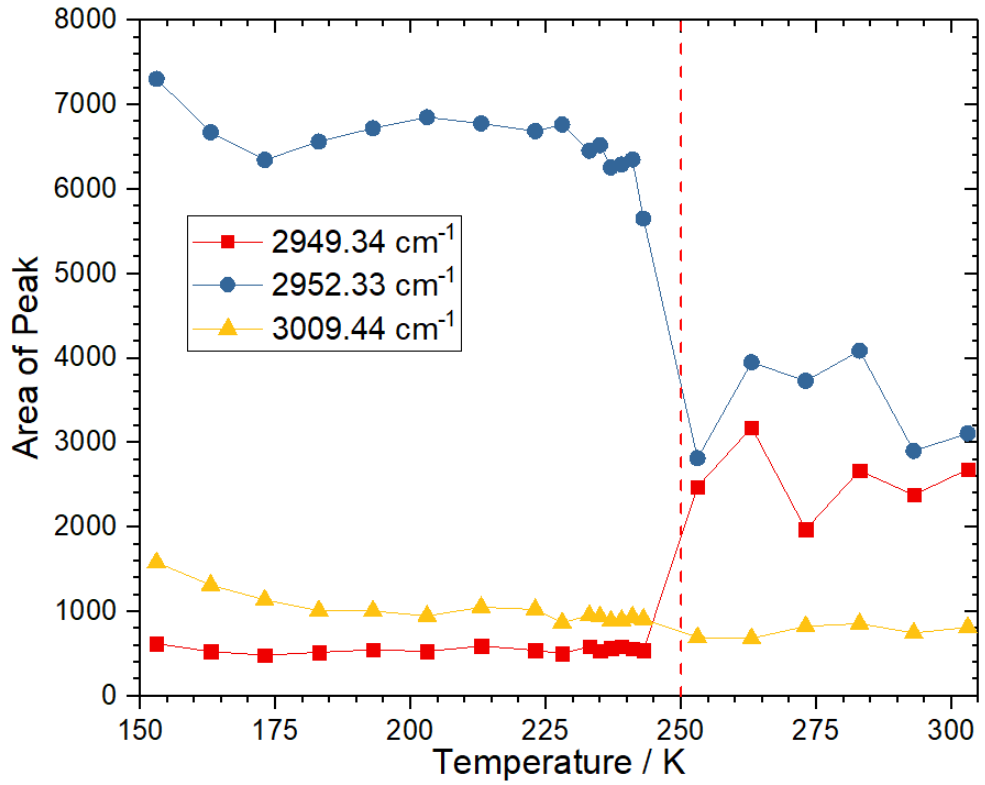

Figure 22: Temperature dependence of the area of the peak for some phonons in $DMA_7Pb_4Br_{15}$

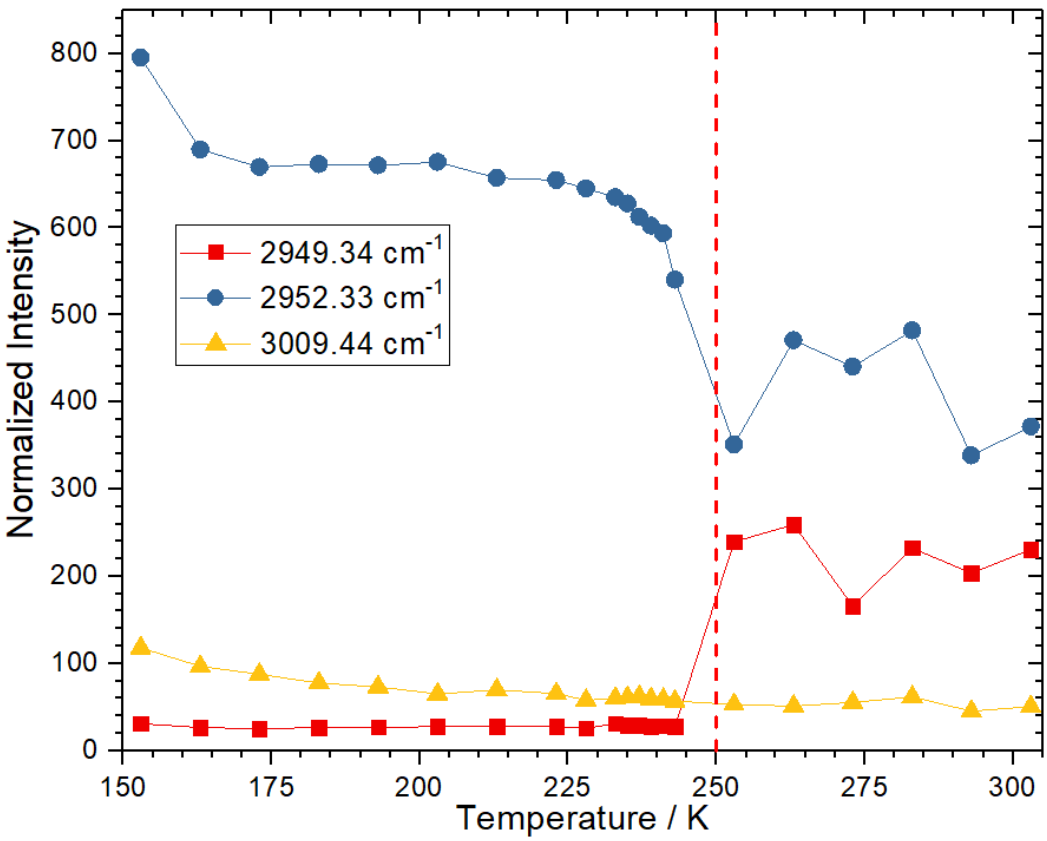

Finally, as was described in Figure 23, some phonons present a modification in the position at 250 K that is the SPT temperature, these particular vibrations are related to 2949.34 and 2952.33 cm^{-1}, after saw the particular behavior was designed the evolution of the FWHM, area, and intensity of the modes for a better-defined transition, these analyses were also compared with one vibration who do not have important temperature variation (3009.44 cm^{-1}). These phonons are linked to a DMA cation ordering movement (CH_3 stretching groups) that easily leads to an increase in H-bounds strength and are exhibit as abrupt changes in all past commented parameters.

Conclusions

Hybrid lead halide perovskites exhibit promising properties, the impact of these compounds has increased due to the discoveries and novel device concepts for using different types of applications. The synthesized compounds with dimethylammonium $[(CH_3)_2NH_2]^+$ (DMA) has amazing possible optoelectronic properties because this organic cation is highly responsible for ordering in the crystal structure, and in most cases responsible for the ferroelectric order. In this context, in this work, we successfully investigated two-hybrid lead halide types like perovskites structures, both of them based on the ABX_3 basic chemical formula.

One compound was the three-dimensional hybrid perovskite $DMAPbBr_3$, the structure exhibit a hexagonal crystal system with a = 8.6159(5) Å, b = 8.6159(5) Å, c = 14.6256(12) Å, γ=120 ° as cell parameters and space group of $P6_3/mmc$ with four molecules per unit cell. The main character is this structure is that it shows infinite constitutional chains of face-sharing $[PbBr_6]^{4-}$ octahedra along the c axis. Each chain is formed by $[Pb_2Br_9]^{5-}$ units, which is formed by two octahedra bounded by a common face, connecting three bromide ions. The units are connected along the chain by an octahedron corner. Thus in the unit cell, there are two units, which are stacked along the c axis forming all chain. On the other hand, the DMA cations are in the cavities left by the chains in two different crystalline sites and isotropically disordered in both. The first DMA position is around the unit cell corners and the second one is around the position (1/3; 2/3; 1/4), in Raman we assigned all the phonon in room temperature of the compound separating the organic DMA part and octahedral $[PbBr_6]^{4-}$ composition.

The low-temperature studies in the $DMAPbBr_3$ material shown that hybrid perovskite $DMAPbBr_3$ exhibits at 250 K a first-order phase transition from hexagonal $P6_3/mmc$ to orthorhombic $P2_12_12_1$ system, where the mechanism of an order-disorder process is involved; In this context, as we demonstrated the DMA^+ cations are dynamically disordered, because they are in high symmetry site position at 300 K for a low symmetric molecule, for this reason, the H-bound in the CH_3 and NH_2 groups cannot reproduce a well-defined molecule, the crystal structure dynamic in low-temperature permits that this organic composition migrate to a better location distorting the crystal base and modifying the crystal structure. Another important factor in low-temperature results is that the decrease of temperature leads to an increase H-bounds strength that in vibrational frequencies and FWHM exhibit abrupt changes. This particular distortion in

the framework can possibly have ferroelastic applications in the compound, another perspective in this composition is the definition of possible the soft mode around 30 cm^{-1}, for these analyses we hope to perform in triple-spectrometer a better Raman spectra that corroborate our initial spectroscopic result, because weak anomalies in the temperature dependence of vibrational frequencies could describe this type of transition. At this instance, optical properties as electrical measurement could be done in this composition for improved characterization of the compound and define potential properties of the hybrid perovskite.

By the other hand, we successfully produce the $DMA_7Pb_4Br_{15}$ crystal and with our SCXRD measurement showed that our crystalline structure is congruent with the literature results, also was described with this technique an isostructural phase transition behavior in the compound at 250 K, 200 K and 180 K temperatures, that are compatible with some reports, the Raman spectroscopy measurements under temperature reveal at 250 K an order-disorder transition in the material, because as $DMAPbBr_3$ compound at high frequencies a temperature dependence of the half-widths, center, area and intensity of some bands in the spectral shown a immediate change in this temperature, resulting in well defined transition at high frequencies. This material posse a novel related chemical formula A_7PbX_{15} and a two-dimensional perovskite, this 2D composition represent a unique physical and chemical properties arising from the quantum confinement effect that promising for optoelectronic characteristics, for these motive techniques that reveal information as PL or bandgap will expose this application.

Our results, in the scientific community, have some impact on the description of the properties and mechanism of the phase order-disorder phase transition. Also, describe a novel phase crystal transition in a hybrid compound with possible, hoping applications. Furthermore, more significant analyses could be carried on in these compositions because has hopeful characteristics and a lot of advantages as an easy synthesized method and cheap materials and low-temperature formation.

Bibliography

BAY, T. et al. Nomenclature of the perovskite supergroup : A hierarchical system of classification based on crystal structure and composition. **Mineralogical Magazine**, v. 81, n. June, p. 411–461, 2017.

BECKER, M.; KLÜNER, T.; WARK, M. Formation of hybrid ABX_3 perovskite compounds for solar cell application: first-principles calculations of effective ionic radii and determination of tolerance factors. **Dalton Transactions**, v. 46, n. 11, p. 3500–3509, 2017.

BESARA, T. et al. Mechanism of the order-disorder phase transition, and glassy behavior in the metal-organic framework $[(CH_3)_2NH_2]Zn(HCOO)_3$. **Proceedings of the National Academy of Sciences**, v. 108, n. 17, p. 6828–6832, 2011.

BHALLA, A. S.; GUO, R.; ROY, R. The perovskite structure: A review of its role in ceramic science and technology. **Materials Research Innovations**, v. 4, n. 1, p. 3–26, nov. 2000.

EAMES, C. et al. Ionic transport in hybrid lead iodide perovskite solar cells. **Nature Communications**, v. 6, n. May, p. 2–9, 2015.

FRISCH, M. J. et al. **Gaussian 09**, 2009.

GARCÍA-FERNÁNDEZ, A. et al. Phase Transition, Dielectric Properties, and Ionic Transport in the $[(CH_3)_2NH_2]PbI_3$ Organic-Inorganic Hybrid with 2H-Hexagonal Perovskite Structure. **Inorganic Chemistry**, v. 56, n. 9, p. 4918–4927, 2017.

GARCÍA-FERNÁNDEZ, A. et al. $[(CH_3)_2NH_2]_7Pb_4X_{15}$ (X = Cl− and Br−), 2D-Perovskite Related Hybrids with Dielectric Transitions and Broadband Photoluminiscent Emission. **Inorganic Chemistry**, v. 57, n. 6, p. 3215–3222, 2018.

GESELLE, M.; FUESS, H. Crystal structure of dimethylammonium tribromoplumbate (II), $(CH_3)_2NH_2PbBr_3$. **Zeitschrift für Kristallographie - New Crystal Structures 212**, n. Ii, p. 6895, 1997.

GRÄTZEL, M. Photoelectrochemical cells. **Nature**, v. 414, n. 6861, p. 338–344, nov. 2001.

GRÄTZEL, M. The light and shade of perovskite solar cells. **Nature Materials**, v. 13, n. 9, p. 838–842, 2014.

HAO, F. et al. Lead-free solid-state organic-inorganic halide perovskite solar cells. **Nature Photonics**, v. 8, n. 6, p. 489–494, 2014.

HUANG, J. et al. Understanding the physical properties of hybrid perovskites for

photovoltaic applications. **Nature Reviews**, v. 2, n. 17042, 2017.

HUTTER, E. M. et al. Direct-indirect character of the bandgap in methylammonium lead iodide perovskite. **Nature Materials**, 2016.

JAIN, P. et al. Order− Disorder Antiferroelectric Phase Transition in a Hybrid Inorganic− Organic Framework with the Perovskite Architecture. **Journal of the …**, v. 130, n. 32, p. 10450–1, 2008.

JODLOWSKI, A. D. et al. Large guanidinium cation mixed with methylammonium in lead iodide perovskites for 19 % efficient solar cells. **Nature Energy**, v. 2, n. 1, p. 972–979, 2017.

JU, D. et al. Gas induced conversion of hybrid perovskite single crystal to single crystal for great enhancement of their photoelectric properties. **Journal of Materials Chemistry A**, v. 5, p. 21919–21925, 2017.

KE, W. et al. Myths and reality of $HPbI_3$ in halide perovskite solar cells. **Nature Communications**, v. 9, n. 1, p. 4785, 2018.

LAN, C. et al. Two-dimensional perovskite materials: From synthesis to energy-related applications. **Materials Today Energy**, v. 11, p. 61–82, 2019.

LEGUY, A. M. A. et al. Dynamic disorder, phonon lifetimes, and the assignment of modes to the vibrational spectra of methylammonium lead halide perovskites. **Physical Chemistry Chemical Physics**, v. 18, n. 39, p. 27051–27066, 2016.

LETIAN DOU et al. Atomically thin two-dimensional organic-inorganic hybrid perovskites. **Science**, v. 349, n. 6255, 2015.

LI, M. et al. Colloidal $CsPbX_3$ (X = Br, I, Cl) NCs: Morphology controlling, composition evolution, and photoluminescence shift. **Journal of Luminescence**, v. 190, n. December 2016, p. 397–402, 2017.

LI, S. et al. Metal Halide Perovskite Single Crystals: From Growth Process to Application. **Crystals**, v. 8, n. 5, p. 220, maio 2018a.

LI, Z. et al. Scalable fabrication of perovskite solar cells. **Nature Reviews**, v. 1, n. 18017, p. 1–20, 2018b.

LIN, H. et al. Low-Dimensional Organometal Halide Perovskites. **ACS Energy Letters**, v. 3, n. 1, p. 54–62, 2018.

MA, Z. et al. Pressure-induced emission of cesium lead halide perovskite nanocrystals. **Nature Communications**, v. 9, n. 1, p. 4506, 2018.

MANCINI, A. et al. Synthesis, structural and optical characterization of $APbX_3$ (A=methylammonium, dimethylammonium, trimethylammonium; X=I, Br, Cl) hybrid

organic-inorganic materials. **Journal of Solid State Chemistry**, v. 240, p. 55–60, 2016.

MCGEHEE, M. D. Materials science: Fast-track solar cells. **Nature**, v. 501, n. 7467, p. 323–325, 2013.

MCGEHEE, M. D. Perovskite solar cells: Continuing to soar. **Nature Materials**, v. 13, n. 9, p. 845–846, 2014.

MOMMA, K.; IZUMI, F. VESTA 3 for three-dimensional visualization of crystal , volumetric and morphology data. p. 1272–1276, 2011.

NAZARENKO, O. et al. Guanidinium-Formamidinium Lead Iodide: A Layered Perovskite-Related Compound with Red Luminescence at Room Temperature. **Journal of the American Chemical Society**, v. 140, n. 11, p. 3850–3853, 2018.

ODENTHAL, P. et al. Spin-polarized exciton quantum beating in hybrid organic-inorganic perovskites. **Nature Physics**, v. 13, n. 9, p. 894–899, 2017.

PEI, Y. et al. Unveiling Property of Hydrolysis-Derived DMAPbI3 for Perovskite Devices: Composition Engineering, Defect Mitigation, and Stability Optimization. **iScience**, v. 15, p. 165–172, 2019.

PETROVIĆ, M.; CHELLAPPAN, V.; RAMAKRISHNA, S. Perovskites: Solar cells & engineering applications – materials device developments. **Solar Energy**, v. 122, p. 678–699, 2015.

QIAN, J. et al. A theoretical study of hybrid lead iodide perovskite homologous semiconductors with 0D, 1D, 2D and 3D structures. **Journal of Materials Chemistry A**, v. 5, n. 32, p. 16786–16795, 2017.

SALIBA, M. et al. Measuring Aging Stability of Perovskite Solar Cells. **Joule**, v. 2, n. 6, p. 1019–1024, 2018.

SAPAROV, B.; MITZI, D. B. Organic-Inorganic Perovskites: Structural Versatility for Functional Materials Design. **Chemical Reviews**, v. 116, n. 7, p. 4558–4596, 2016.

SATO, T. et al. Extending the applicability of the Goldschmidt tolerance factor to arbitrary ionic compounds. **Scientific Reports**, v. 6, n. January, p. 1–10, 2016.

ŠIMÉNAS, M. et al. Electron paramagnetic resonance of a copper doped $[(CH_3)_2NH_2][Zn(HCOO)_3]$ hybrid perovskite framework. **Physical Chemistry Chemical Physics**, p. 12097–12105, 2018.

ŠIMÉNAS, M. et al. Elucidation of dipolar dynamics and the nature of structural phases in the $[(CH_3)_2NH_2][Zn(HCOO)_3]$ hybrid perovskite framework. **Journal of Materials Chemistry C**, v. 7, p. 6779–6785, 2019.

TILLEY, J. D. R. **Perovskites**. First Edit ed. United Kingdom: Wiley, 2016.

TRIGUI, W. et al. Raman study of order-disorder phase transition in $[(C_3H_7)N]_3Bi_3Cl_{12}$ compound. **Journal of Molecular Structure**, v. 1106, p. 19–29, 2016.

TSAI, H. et al. High-efficiency two-dimensional ruddlesden-popper perovskite solar cells. **Nature**, v. 536, n. 7616, p. 312–317, 2016.

VEGA, E.; MOLLAR, M.; MARÍ, B. Effect of guanidinium on the optical properties and structure of the methylammonium lead halide perovskite. **Journal of Alloys and Compounds**, v. 739, p. 1059–1064, 2018.

WEI, H. et al. Dopant compensation in alloyed $CH_3NH_3PbBr_{3-x}Cl_x$ perovskite single crystals for gamma-ray spectroscopy. **Nature Materials**, v. 16, n. 8, p. 826–833, 2017.

WENGER, B. et al. Consolidation of the optoelectronic properties of $CH_3NH_3PbBr_3$ perovskite single crystals. **Nature Communications**, v. 8, n. 1, 2017.

YIN, J. et al. Molecular behavior of zero-dimensional perovskites. **Science Advances**, v. 3, n. 12, p. e1701793, 2017.

ZHANG, C. et al. Magnetic field effects in hybrid perovskite devices. **Nature Physics**, v. 11, n. 5, p. 427–434, 2015.

ZHANG, L.; ZENG, Q.; WANG, K. Pressure-Induced Structural and Optical Properties of Inorganic Halide Perovskite $CsPbBr_3$. **Journal of Physical Chemistry Letters**, v. 8, n. 16, p. 3752–3758, 2017.

ZHANG, Q.; YIN, Y. All-Inorganic Metal Halide Perovskite Nanocrystals: Opportunities and Challenges. **ACS Central Science**, 2018.

Appendix: DFT Raman $[(CH_3)_2NH_2]^+$ molecule calculation

The HIOP organic visualization is less studied for this reason we made a DFT calculation with dimethylammonium $[(CH_3)_2NH_2]^+$ (DMA) molecule in Gaussian09 software. [1] This calculation was to assign vibrational modes of the cation. For these calculations, was used the Opt+Freq in the job type window, also were used a tight convergence criteria, for optimize the molecule to a minimum and compute the Raman spectra, in the method window was used a ground state, DFT, unrestricted and B3LYP functional, with a 6-311G, ++ (d,p) base, a charge equal 0 and singlet spin. In the general part, we ignored the symmetry of the molecule and was calculated the Hirshfeld (CM5) charges. In this Appendix is showed the results of this DFT simulation of Raman spectra. The optimized DMA calculation molecule is showed in Figure **18**, where are described each element blue for Nitrogen (N), gray for Carbon (C) and white for Hydrogen (H).

Figure 23: Dimethylammonium $[(CH_3)_2NH_2]^+$ (DMA) molecule view of DFT optimization

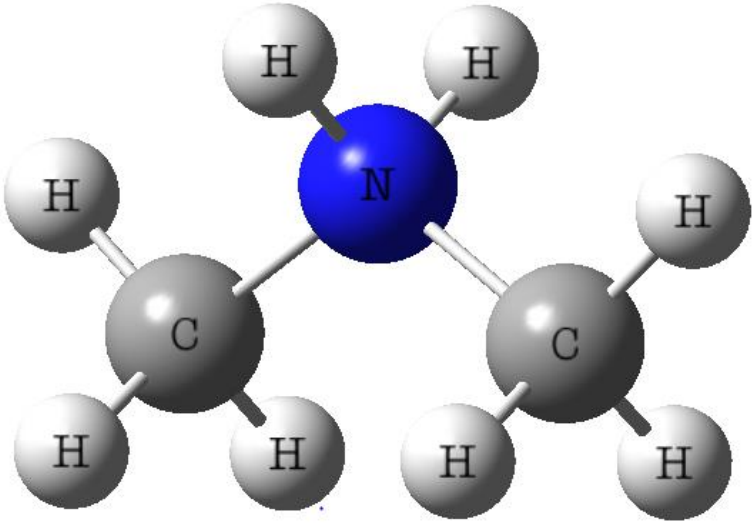

Also, the molecule information for $[(CH_3)_2NH_2]^+$ cation is: (a) The atomic charges Mulliken type is 0.2920 for N, 0.0024 for C, for the H bounded with carbon are 0.0520 and (b) for the ones with is -0.317. For bonds the distance between C-H is 1.09 Å, C-N is 1.50 Å and N-H 1.05 Å.

The simulated Raman of the molecule DMA was calculated with a frequency optimization between (0-3200) cm^{-1} with the past calculation description. In Figure **19** is showed Raman spectrum for dimethylammonium molecule, in the graph, the intensity

was normalized, each peak was assigned with a red line below to determine the exact frequency value, the complete spectrum has 27 actives modes and finally was highlight the (0-1600) cm^{-1} range to follow a better appreciation of assigned.

Figure 24: Normalized dimethylammonium $[(CH_3)_2NH_2]^+$ (DMA) molecule Raman spectra calculated by DFT calculation in Gaussian09 software.

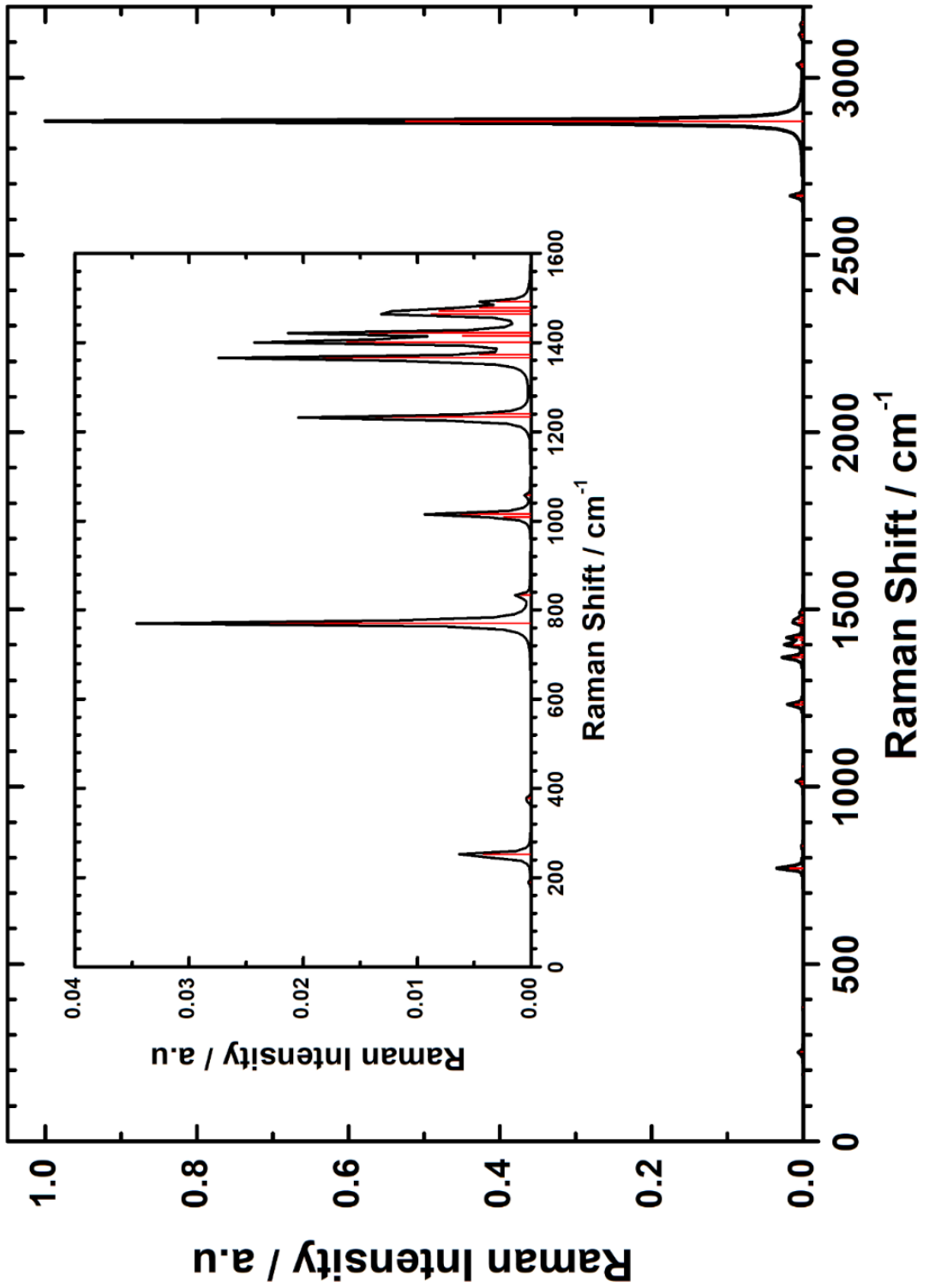

The values for the assignment of each vibrational mode of DMA cation are included in Table 5, also with a few information about the position of each peak in frequency, the Raman intensity activity, Raman normalized intensity, and a description of each type of movement vibration compared to the ones described in the literature. [2,3]

Table 5: Simulated frequencies and intensities of the Raman peaks of the DMA molecule.

Mode Number	Frequency (cm^{-1})	Raman Intensity Activity (a.u)	Raman Normalized Intensity (%)	Description
1	188.9030	24.4217	0.0124	$\rho_{as}(CH_3)$
2	249.6882	893.8050	0.4535	$\rho_s(CH_3)$; $\rho(NH_2)$
3	374.9386	76.6455	0.0389	$\omega(CH_3)$
4	771.0545	4405.6876	2.2355	$\tau(CH_3)$; $\rho(NH_2)$
5	831.0575	191.4654	0.0972	ν_s(C-N-C)
6	1007.2550	4.7312	0.0024	ν_{as}(C-N-C); $\omega(CH_3)$
7	1013.5494	1327.2146	0.6734	$\tau_{as}(CH_3)$; $\tau(NH_2)$
8	1055.8152	72.2331	0.0367	ν_{as}(CNC); $\omega(NH_2)$
9	1230.6839	2863.8303	1.4531	$\omega(CH_3)$
10	1237.3043	295.1687	0.1498	$\tau_s(CH_3)$; $\tau(NH_2)$
11	1363.5052	4134.5139	2.0979	$\tau(NH_2)$
12	1370.2386	96.3383	0.0489	$\omega_s(CH_3)$; $\omega(NH_2)$
13	1402.0607	4003.1014	2.0312	$\delta_s(NH_2)$
14	1414.6414	48.1154	0.0244	$\omega_{as}(CH_3)$; $\omega(NH_2)$
15	1420.5244	2745.0308	1.3928	$\omega_{as}(CH_3)$; $\delta_s(NH_2)$
16	1466.2218	2854.3473	1.4483	τ_{as} (CH_3)
17	1477.0993	521.9316	0.2648	$\delta_s(CH_3)$
18	1482.2715	24.7953	0.0126	$\tau_s(CH_3)$
19	1490.3221	511.7455	0.2597	$\delta_s(CH_3)$; $\delta_s(NH_2)$
20	2666.0272	3330.3602	1.6898	$\nu_{as}(NH_2)$
21	2876.6249	197080.4223	100	$\nu_s(NH_2)$
22	3034.3830	1212.6679	0.6153	$\nu_s(CH_3)$
23	3037.6901	911.6117	0.4626	$\nu_{as}(CH_3)$
24	3117.8556	924.6201	0.4692	$\nu_s(CH_3)$
25	3124.1839	709.8868	0.3602	$\nu_{as}(CH_3)$
26	3142.5367	54.6766	0.0277	$\nu_{as}(CH_3)$
27	3148.0519	778.7344	0.3951	$\nu_{as}(CH_3)$

Abbreviations: as asymmetric; s: symmetric; ν: stretching; δ: in-plane bending; τ: twisting; ρ: rocking; ω: wagging.

Figure 25: Schematic representation of the vibrational modes of the phonon of dimethylammonium $[(CH_3)_2NH_2]^+$ (DMA) molecule. For (a) the first 14 modes and (b) last 13 ones.

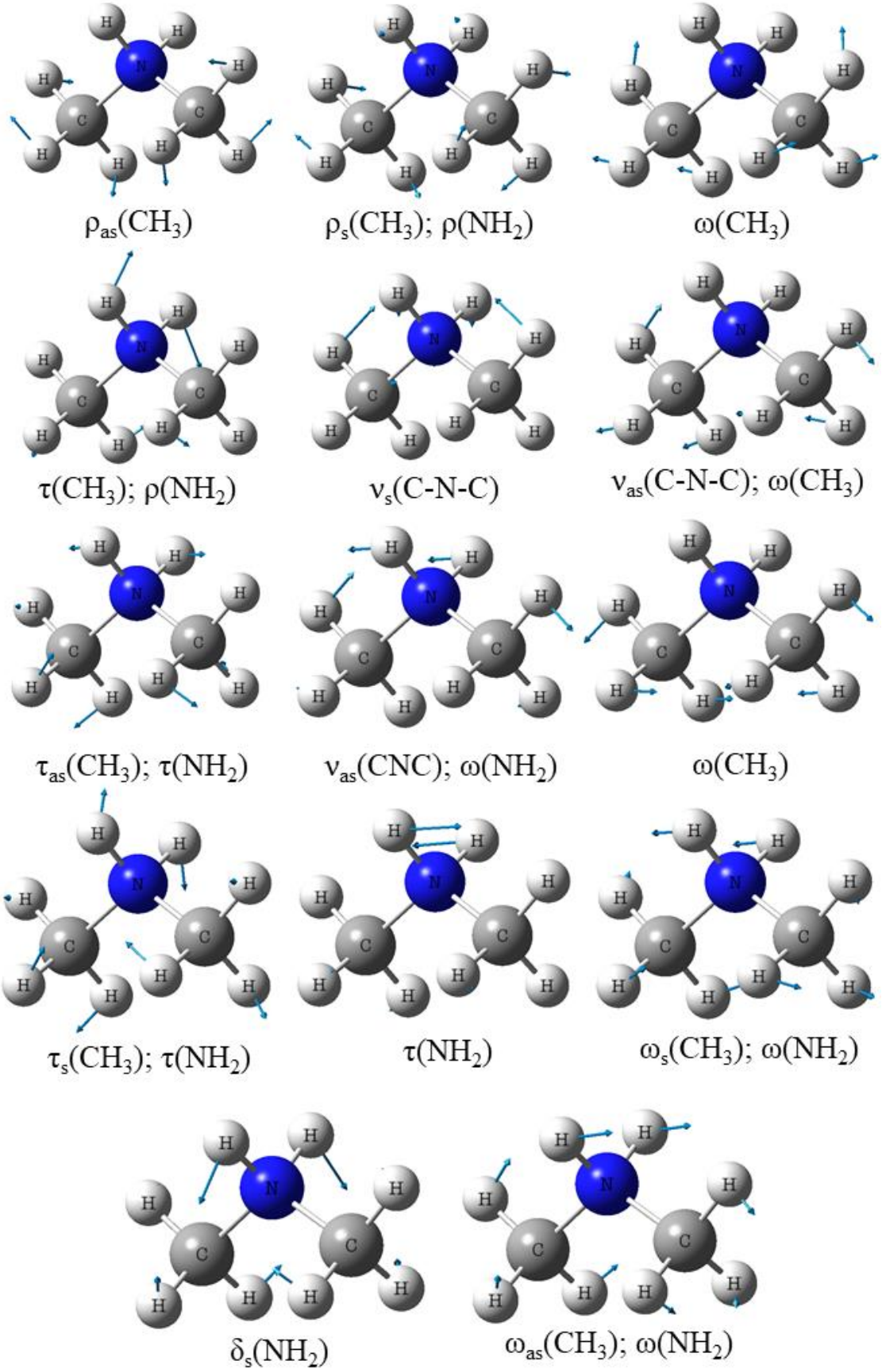

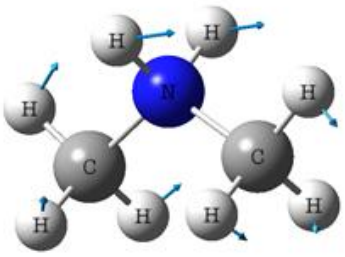

$\omega_{as}(CH_3)$; $\delta_s(NH_2)$

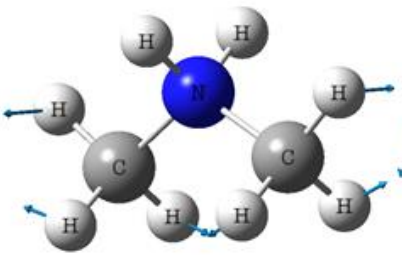

τ_{as} (CH_3)

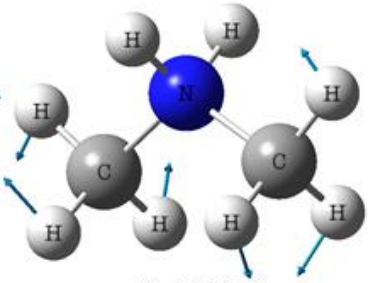

$\delta_s(CH_3)$

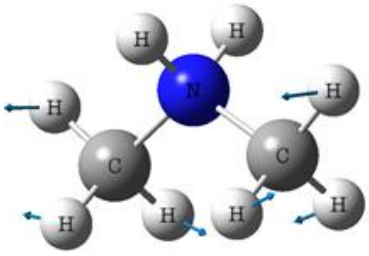

$\tau_s(CH_3)$

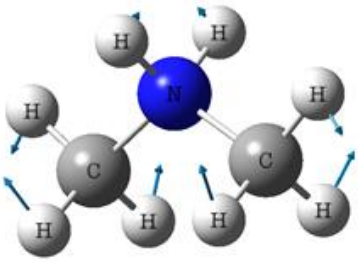

$\delta_s(CH_3)$; $\delta_s(NH_2)$

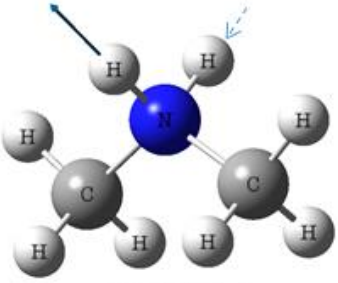

$\nu_{as}(NH_2)$

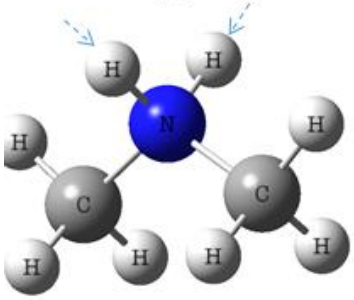

$\nu_s(NH_2)$

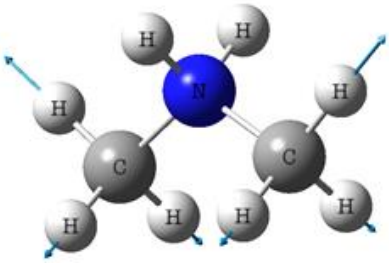

$\nu_s(CH_3)$

$\nu_{as}(CH_3)$

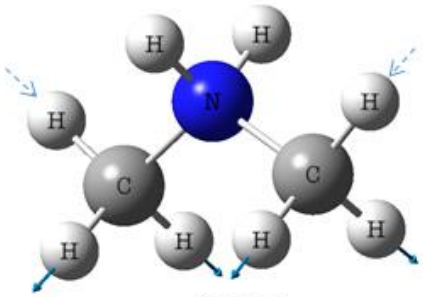

$\nu_s(CH_3)$

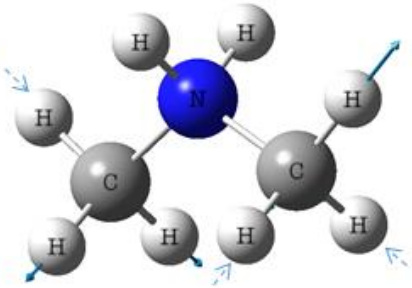

$\nu_{as}(CH_3)$

$\nu_{as}(CH_3)$

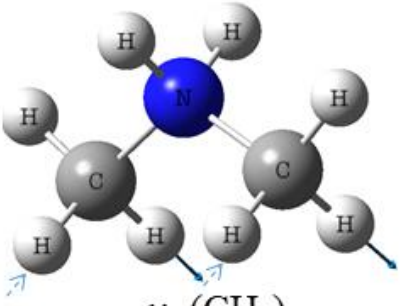

$\nu_{as}(CH_3)$

References

1. M. J. Frisch, G. W. Trucks, H. B. Schlegel, G. E. Scuseria, M. A. Robb, J. R. Cheeseman, G. Scalmani, V. Barone, B. Mennucci, G. A. Petersson, H. Nakatsuji, M. Caricato, X. Li, H. P. Hratchian, A. F. Izmaylov, J. Bloino, G. Zheng, J. L. Sonnenberg, M. H. Gaussian 09. Revision E.01 (2009).
2. Qian, J., Guo, Q., Liu, L., Xu, B. & Tian, W. A theoretical study of hybrid lead iodide perovskite homologous semiconductors with 0D, 1D, 2D, and 3D structures. *J. Mater. Chem. A* **5,** 16786–16795 (2017).
3. Mączka, M., Zierkiewicz, W., Michalska, D. & Hanuza, J. Vibrational properties and DFT calculations of the perovskite metal formate framework of $[(CH_3)_2NH_2][Ni(HCOO_3)]$ system. *Spectrochim. Acta - Part A Mol. Biomol. Spectrosc.* **128,** 674–680 (2014).